Journal of Computational Physics 299 (2015) 1–21

Contents lists available at ScienceDirect

Journal of Computational Physics

www.elsevier.com/locate/jcp

Dispersion relation equation preserving FDTD method for nonlinear cubic Schrödinger equation

Tony W.H. Sheu [a,b,c,*], Le Lin [a]

[a] Department of Engineering Science and Ocean Engineering, National Taiwan University, Taipei, Taiwan
[b] Institute of Applied Mathematical Sciences, National Taiwan University, Taipei, Taiwan
[c] Center for Advanced Study in Theoretical Sciences, National Taiwan University, Taipei, Taiwan

ARTICLE INFO

Article history:
Received 8 July 2014
Received in revised form 22 May 2015
Accepted 18 June 2015
Available online 3 July 2015

Keywords:
Cubic Schrödinger equation
Method of fractional steps
Four temporal steps
Explicit symplectic scheme
Dispersion relation equation

ABSTRACT

In this study we aim to solve the cubic nonlinear Schrödinger (CNLS) equation by the method of fractional steps. Over a time step from t_n to t_{n+1}, the linear part of the Schrödinger equation is solved firstly through four time integration steps. In this part of the simulation, the explicit symplectic scheme of fourth order accuracy is adopted to approximate the time derivative term. The second-order spatial derivative term in the linear Schrödinger equation is approximated by centered scheme. The resulting symplectic and space centered difference scheme renders an optimized numerical dispersion relation equation. In the second part of the simulation, the solution of the nonlinear equation is computed exactly thanks to the embedded invariant nature within each time increment. The proposed semi-discretized difference scheme underlying the modified equation analysis of second kind and the method of dispersion error minimization has been assessed in terms of the spatial modified wavenumber or the temporal angular frequency resolution. Several problems have been solved to show that application of this new finite difference scheme for the calculation of one- and two-dimensional Schrödinger equations can deemed conserve Hamiltonian quantities and preserve dispersion relation equation (DRE).

1. Introduction

Nonlinear Schrödinger equation (NLS) governs wave propagation for example in fiber [1] and in deep water [2]. This practically and scientifically important equation has been extensively studied in the past through either a theoretical or a computational approach to explore its rich quantum-mechanical behaviors. A better understanding of the nonlinear nature of this equation is in particular essential to design modern nanoscale semiconductors, quantum dot device and quantum cellular automata.

In addition to the existence of many fruitful physics phenomena in solitary waves, Schrödinger equation has some remarkable mathematical features as well. This completely integrable equation belongs to the Hamiltonian class of differential equations. Being a Hamiltonian equation, Schrödinger equation permits an infinite number of conserved quantities. Because of the presence of these mathematical invariants, Schrödinger equation conserves charge, momentum, energy, and other quantities consisting of higher-order spatial derivative terms. Apart from a numerous integral conserved nature, the local

* Corresponding author at: Department of Engineering Science and Ocean Engineering, National Taiwan University, Taipei, Taiwan. Tel.: +886 2 33665746; fax: +886 2 23929885.
E-mail address: twhsheu@ntu.edu.tw (T.W.H. Sheu).

http://dx.doi.org/10.1016/j.jcp.2015.06.023
0021-9991/

conserved energy and the momentum quantities can be also theoretically derived from the Schrödinger equation. By means of the Legendre transformation, the Cauchy problem of the Schrödinger equation can be transformed to its counterpart consisting of the Hamiltonian canonical equations. One can refer to [3,4] to get some distinguished mathematical properties embedded in the currently investigated cubic NLS (CNLS) equation.

Thanks to many theoretical features mentioned above in the Schrödinger equation, it is better that we take all of them into consideration while solving its associated Cauchy problem so as to be able to obtain a physically more accurate solution at late time. We are therefore aimed to develop a scheme accommodating geometric structure so as to numerically preserve symplecticity in the Hamiltonian type of Schrödinger equation. Development of a geometric numerical scheme is particularly essential while solving the time-dependent Schrödinger equation over a long time span. Otherwise, all the conserved quantities existing in the Hamiltonian equation, which is of current interest, cannot be satisfied numerically. In addition to preserving the discrete geometric structure in the approximation of Schrödinger equation by employing a symplectic temporal scheme, it is equally important to preserve its phase or group velocity numerically. Otherwise, a train of NLS wave solutions will be erroneously predicted after a long simulation time. Moreover, in numerical simulations unphysical oscillations near sharp wave fronts may appear. In this light, a scheme developed for the spatial derivative terms should preserve wave phase, group velocity, modified wavenumber, and an even important property known as the dispersion relation equation. For an overview of the numerical methods in the literature, one can refer to [5].

It has been known for a while that the solution of Korteweg–de Vries (*KdV*) equation remains smooth all the time provided that in this equation the coefficient of the third-order dispersion coefficient is large. On the contrary, *KdV* equation permits discontinuous solution in the zero-dispersion limit regardless of the initially prescribed smooth solution [6]. The deteriorated smoothness in the predicted solution resulting from the reduced dispersion or even from the formation of shock-like solution in the limit of zero dispersion can be also observed, for example, in the NLS equation. Inclusion of the dispersion term to the wave equation can prevent shock formation, which has been an academic topic of many intensive studies. Like the *KdV* equation investigated at its zero-dispersion limit, the present study of the NLS equation is also focused on the case with a fairly small dispersion coefficient. Numerical investigation of the effect of dispersive term on the solution smoothness and on the breaking of wave solution from a focusing state to an oscillatory state is one of the objectives of the present study.

One of the most important dynamical features reported in the numerical study of NLS equation is the formation of modulational instability (MI) phenomenon [2]. This type of instability arises from an anomalously predicted group/phase velocity dispersion. Under this circumstance, a pulse of shorter wavelength travels with a larger group/phase velocity than a pulse with longer wavelength [7]. The resulting onset of the MI leads to spectral sidebands [2]. These erroneously predicted sidebands may be amplified further by the nonlinear term in Schrödinger equation. As a consequence, the waveform will be eventually broken into a train of pulses [8]. Development of a dispersion error reducing scheme is therefore a crucial step to eliminate the so-called modulational instability.

In solid-state physics, many studies require getting an accurate solution of the Schrödinger equation investigated at a fairly small scaled Planck constant. The applicability of the proposed scheme to solve the Schrödinger equation effectively in the semiclassical regime (i.e., for small-scaled Planck constant) is of utmost importance. This computational challenge motivates us to develop a new dispersion error reducing and numerically stable difference scheme for the calculation of Schrödinger equation in semiclassical regime. Provided that the scaled Planck constant is small, Schrödinger equation is known to propagate oscillations of wavelength with an order of Planck constant. The presence of such an oscillatory solution nature in the simulation prevents Schrödinger solution from converging strongly as the scaled Planck constant ε (shown later in equation (3)) approaches zero, thereby resulting in a severe computational difficulty [9]. Markowich et al. [10] pointed out that both of the grid spacing and the time increment must be chosen to be an order of ε for getting a good approximation of the Schrödinger equation. This subject will be discussed in this study as well.

The rest of the paper is organized as follows. In Section 2 the cubic NLS equation cast in differential form is presented along with some of its mathematically rich properties. The four-stage fourth-order accurate explicit symplectic time integrator is then presented in Section 3.1.1 for the approximation of temporal derivative term within the semi-discretization framework. In Section 3.1.2, the spatial derivative terms are properly approximated with an aim to obtain a better dispersive numerical behavior. Our strategy is to preserve numerical dispersion relation equation by minimizing the derived discrepancy between the numerical and exact dispersion relation equations. Following the method of fractional steps, the NLS solver presented in Section 3 is applied to solve the two-dimensional cubic NLS equation in Section 4. The Cauchy problems amenable to exact solutions are then solved in Section 5 to verify the proposed dispersion-relation-equation- and symplecticity-preserving scheme. Important numerical insights of the newly developed explicit scheme for solving the self-focusing cubic NLS equation are also revealed. Finally, in Section 6 we conclude this study based on the simulated results.

2. Governing equation and its mathematical properties

The following wave equation describes the non-realistic quantum mechanics for spinless particles of mass m moving in a field subject to the potential function V_0 [11]

$$\imath\hbar\psi_t = -\frac{\hbar^2}{2m}\nabla^2\psi + V_0(x,t)\psi. \tag{1}$$

In the above time-dependent Schrödinger equation, $\hbar$ denotes the Planck's constant and ψ is a complex amplitude (or envelop) of the wave packet under investigation. The above equation is normalized by $T = 2mL^2/\hbar$ and L, where L and T are the characteristic length and time, respectively. The corresponding dimensionless Schrödinger equation is derived as

$$\imath\psi_t + \psi_{xx} + V(x,t,|\psi|^2)\psi = 0, \tag{2}$$

where $\imath = \sqrt{-1}$.

By changing the variables from $\psi(x,t)$ to $u(x^*,t^*)$, one can rewrite equation (2) into a form of semiclassical Schrödinger equation. This transformed equation involves the scaled Planck's constant ε, where $0 < \varepsilon \ll 1$, as

$$\imath\varepsilon u_{t^*} + \frac{\varepsilon^2}{2}u_{x^*x^*} + V(x^*,t^*,|u|^2)u = 0. \tag{3}$$

In the above, $x^* = \sqrt{\varepsilon}x$, $t^* = 2t$ and $u = \sqrt{\varepsilon}\psi$ [6]. Through the mapping from (x,t) to (x^*,t^*), the spatial domain has been found to be amplified by a factor of $\sqrt{\varepsilon}$. Schrödinger equation expressed in (x^*,t^*) coordinates facilitates us to numerically solve it and capture the phenomena of propagation under such a subtle scale.

The sign of the nonlinear term V in equation (2) corresponds to the focusing (for $V > 0$) and defocusing (for $V < 0$) NLS equations, respectively. Equation (2) is a generic model used frequently to describe the evolution of an envelope wave in nonlinear dispersive medium. Simulation of electromagnetic waves in optical fiber, deep water waves, and Langmuir waves in plasmas involves solving the NLS equation. Many other applications of the NLS equation can be found in [12].

In this study, the solution of one-dimensional Schrödinger equation is sought subject to the potential $V = 2|\psi|^2$, thereby yielding the following dimensionless Schrödinger equation with the cubic nonlinear term

$$\imath\psi_t + \psi_{xx} + 2|\psi|^2\psi = 0. \tag{4}$$

The above CNLS (Cubic NLS) equation is rescaled to the following focusing nonlinear Schrödinger (FNLS) equation through the transformation of equation

$$\imath\varepsilon u_{t^*} + \frac{\varepsilon^2}{2}u_{x^*x^*} + |u|^2u = 0. \tag{5}$$

The small positive scaled Planck's constant ε shown above is used to measure the relative dominance of the terms accounting for the dispersion and nonlinearity. All the superscripts "$*$" shown above have been omitted for simplicity.

Given an initial condition $u_0(x, t=0)$ with the norm $|u_0|^2$ for the intensity power of electromagnetic field slightly lager than a threshold value, equation (5) can self-focus and may become singular in finite time [13]. The physical quantity known as the electric field amplitude, for example, is not infinite in magnitude, implying the break of equation (4) near singularity. The above equation with self-focusing nonlinearity will be solved subject to the periodic boundary condition.

The complex-valued equation (4) is reformulated below within the context of its real-valued counterparts by decomposing ψ into the real functions p and q as follows

$$\psi = p + q\imath. \tag{6}$$

Having split the wave amplitude ψ into the above two parts, we define the solution vector as $\underline{z} = (p,q)^T$. The corresponding equation for (4) can be now expressed in terms of H as [3,14]

$$d\underline{z}/dt = \underline{\underline{J}}\,\delta H(\underline{z})/\delta\underline{z}, \tag{7}$$

where $\underline{\underline{J}} = \begin{pmatrix} 0 & 1 \\ -1 & 0 \end{pmatrix}$. The Hamiltonian H shown above for the investigated CNLS equation is

$$H = \frac{1}{2}\int p_x^2 + q_x^2 - (p^2+q^2)^2 dx. \tag{8}$$

Thanks to equation (8), we can now express H as the sum of the kinetic energy H_1 and the potential energy H_2 shown below [5]

$$H = H_1(p) + H_2(q) = \frac{1}{2}(\underline{p}^T\underline{\underline{U}}\,\underline{p} + \underline{q}^T\underline{\underline{V}}\,\underline{q}). \tag{9}$$

In the above, $\underline{\underline{U}}$ is a symmetric positive definite matrix and $\underline{\underline{V}}$ is equal to its transport $\underline{\underline{V}}^T$. Given the solution variables p, q and the above Hamiltonian, Schrödinger equation can be rewritten as the canonical system of equations given as $\frac{dp}{dt} \equiv \dot{p} = -\frac{\delta H}{\delta q} = -\frac{\delta H_2(q)}{\delta q}$ and $\frac{dq}{dt} \equiv \dot{q} = \frac{\delta H}{\delta p} = \frac{\delta H_1(p)}{\delta p}$ [5]. The solution variables p and q are known, respectively, as the canonical coordinates and the conjugate canonical momentum [15,16]. These canonical equations can be rewritten equivalently as $p_t = -f(q,t)$ and $q_t = g(p,t)$, where $f = q_{xx} + 2(p^2+q^2)q$ and $g = p_{xx} + 2(p^2+q^2)p$ [5].

Equation (4) subject to a given initial solution $\psi_0(x)$ constitutes the so-called Cauchy problem. Its unique solution satisfies the expression indicating the existence of the conserved charge given below [17]

$$F_1 = \int_{-\infty}^{\infty} |\psi(x,t)|^2 dx = \int_{-\infty}^{\infty} |\psi_0(x)|^2 dx. \tag{10}$$

One-dimensional CNLS equation is completely integrable and has therefore infinitely many invariants. Amongst the conserved quantities which can be derived by the technique involving the Lax pair equations, the expressions given by

$$F_2 = \int_{-\infty}^{\infty} \{\psi \frac{d\overline{\psi}}{dx} - \overline{\psi}\frac{d\psi}{dx}\} dx \tag{11}$$

and

$$F_3 = \int_{-\infty}^{\infty} \{2|\frac{d\psi}{dx}|^2 - 2|\psi|^4\} dx \tag{12}$$

are known to indicate the global conserved momentum and energy, respectively. In equation (11), $\overline{\psi}$ denotes the complex conjugate of ψ. Other conserved quantities used later in this article for the code verification purpose are summarized below [18]

$$F_4 = \int_{-\infty}^{\infty} \{2\frac{d\overline{\psi}}{dx}\frac{d^2\psi}{dx^2} - 6|\psi|^2\overline{\psi}\frac{d\psi}{dx}\} dx, \tag{13}$$

$$F_5 = \int_{-\infty}^{\infty} \{2|\frac{d^2\psi}{dx^2}|^2 - 12|\psi|^2|\frac{d\psi}{dx}|^2 - 2(\frac{d|\psi|^2}{dx})^2 + 4|\psi|^6\} dx, \tag{14}$$

$$F_6 = \int_{-\infty}^{\infty} \{2\frac{d^2\overline{\psi}}{dx^2}\frac{d^3\psi}{dx^3} - 10|\frac{d\psi}{dx}|^2\frac{d|\psi|^2}{dx} - 20|\psi|^2\frac{d\overline{\psi}}{dx}\frac{d^2\psi}{dx^2} + 20|\psi|^4\overline{\psi}\frac{d\psi}{dx}\} dx. \tag{15}$$

All equations (10)–(15) for these conserved quantities are useful for us to indirectly verify the numerical method proposed in Section 5 while solving the Schrödinger equation.

We define firstly two new variables $v = q_x$ and $w = p_x$. The CNLS equation can then be rewritten to its equivalent local conservative form $\frac{\partial E(z)}{\partial t} + \frac{\partial F(z)}{\partial x} = 0$, where E $(\equiv \frac{1}{2}[(p^2+q^2)^2 - (v^2+w^2)])$ represents the energy and $F(\underline{z})$ $(\equiv wp_t + vq_t)$ denotes the energy flux [19]. By defining the momentum as $I(\underline{z}) = \frac{1}{2}(pv - qw)$ and the momentum flux as $G(\underline{z}) = \frac{1}{2}[v^2 + w^2 + (p^2+q^2)^2] - \frac{1}{2}(pq_t - qp_t)$, the CNLS equation can be rewritten to the equation that is identical to the local momentum conservative form $\frac{\partial I(z)}{\partial t} + \frac{\partial G(z)}{\partial x} = 0$ [19,20]. The other conservative form given by $N_t + M_x = 0$ in [21] exists for the CNLS equation as well, where $N = \frac{1}{2}(p^2+q^2)$ and $M = pq_x - qp_x$. In this study, these conservative natures are employed as our guidelines to check whether or not the Schrödinger solutions have been correctly computed in Section 5.

While solving the infinite dimensional Hamiltonian system of CNLS equations, the method of lines is chosen to achieve the goal of obtaining a solution of higher quality. Within the resulting semi-discretization framework, application of a mathematically appropriate temporal scheme presented in Section 3.1.1 enables us to retain the symplectic geometric structure in the Schrödinger equation. The second-order spatial derivative term is approximated by the centered difference scheme described in Section 3.1.2. While solving partial differential equations by finite difference time domain (FDTD) methods, it is essential to ensure scheme stability and, at the same time, to reduce numerical dispersion error. Our underlying methodology chosen to reduce dispersion error in five-point stencil is to minimize the derived difference between the numerical and exact dispersion relation equations.

3. Two-step Schrödinger equation solver

The dimensionless CNLS equation (4) will be solved through two steps following the work of Bao et al. in [9]. In the first solution step, the linear equation given below is solved

$$\imath\psi_t + 2\psi_{xx} = 0. \tag{16}$$

Calculation of the solution ψ for equation (4) is followed by solving the following nonlinear equation

$$\imath\psi_t + 4|\psi|^2\psi = 0. \tag{17}$$

Application of the above linear–nonlinear splitting approach renders, however, a first-order accuracy in time [22]. From a time stage $t = t^n$ to $t = t^{n+1}$, the linear equation (16) will be solved using the four-stage fourth-order accurate explicit symplectic Partitioned Runge–Kutta (PRK) scheme described in Section 3.1.1. The dispersion-relation-equation-preserving scheme is then developed for the first time, to the best of authors' knowledge, to approximate spatial derivative term in Section 3.1.2. The reason for applying the temporally first order accurate linear–nonlinear time-splitting method is that the solution of the nonlinear equation (17) can be solved exactly in Section 3.2 thanks to the invariant value of $|\psi|^2$. In addition, we can get the long-time Hamiltonian preserving solution from equation (16).

3.1. Numerical method for the linear Schrödinger equation

A pair of conjugate momenta $v = q_x$ and $w = p_x$ is introduced to rewrite the canonical linear Schrödinger equation to the following system of first-order differential equations

$$p_t + v_x = -2(p^2 + q^2)q, \tag{18}$$

$$-q_t + w_x = -2(p^2 + q^2)p. \tag{19}$$

The above set of equations is identical to the multi-symplectic Hamiltonian differential system given as $\underline{\underline{M}}\underline{\bar{z}}_t + \underline{\underline{K}}\underline{\bar{z}}_x = \nabla S(\underline{\bar{z}})$, where $\underline{\bar{z}} = (p, q, v, w)^T$ and $S(\underline{\bar{z}}) = \frac{1}{2}(v^2 + w^2 + \frac{1}{2}(p^2 + q^2)^2)$ [3]. The two matrices shown above are expressed as $\underline{\underline{M}} = \begin{pmatrix} 0 & 1 & 0 & 0 \\ -1 & 0 & 0 & 0 \\ 0 & 0 & 0 & 0 \\ 0 & 0 & 0 & 0 \end{pmatrix}$ and $\underline{\underline{K}} = \begin{pmatrix} 0 & 0 & -1 & 0 \\ 0 & 0 & 0 & -1 \\ 1 & 0 & 0 & 0 \\ 0 & 1 & 0 & 0 \end{pmatrix}$.

Since equations (4) and (16) possess multi-symplectic structure, any numerical method capable of preserving, for example, symplecticity and invariant should be adopted. In comparison with the conventional numerical integrators, application of geometric numerical discretization methods enables us to get the Schrödinger solution with an improved accuracy and an enhanced stability [20,21]. We are therefore prompted to adopt the method of lines to discretize the Hamiltonian partial differential equation.

In this study, the spatial derivative term ψ_{xx} is approximated firstly by the five-point centered scheme given below

$$\psi_{xx} = \frac{\gamma\psi_{i-2} + (1-4\gamma)\psi_{i-1} + (6\gamma-2)\psi_i + (1-4\gamma)\psi_{i+1} + \gamma\psi_{i+2}}{\Delta x^2} + O(\Delta x^4). \tag{20}$$

The symplectic method described in Section 3.1.1 is then applied to integrate the resulting Hamiltonian ordinary differential equations. Within the semi-discretization context, the introduced coefficient γ shown in equation (20) will be determined in Section 3.1.2.

3.1.1. Symplectic integrator for the temporal derivative term

Either a symplectic or a Poisson type numerical integrator can be employed to conserve the integral invariants in Schrödinger equation. In this study, the explicit symplectic integrator is applied so that the numerical dispersion relation equation can be derived. Besides retaining the embedded symplectic structure in the currently investigated Hamiltonian equation, we are also aimed to get a higher temporal accuracy while solving the linear Schrödinger equation (16). These two objectives in the scheme development can be both achieved using the general s-stage r-order explicit symplectic temporal scheme given in [23]. Not only the symplectic solution structure can be preserved, we can also get a more accurate solution even after a long-time calculation. According to [5], the following four-stage ($s = 4$) fourth-order ($r = 4$) accurate explicit Partitioned Runge–Kutta (PRK) symplectic scheme, which is derived at the coefficients chosen as $c_1 = 0$, $c_2 = c_4 = (2 - 2^{1/3})^{-1}$, $c_3 = 1 - 2(2 - 2^{1/3})^{-1}$, $d_1 = d_4 = \frac{1}{2}(2 - 2^{1/3})^{-1}$ and $d_2 = d_3 = \frac{1}{2}[1 - (2 - 2^{1/3})^{-1}]$, is applied.

First-stage:

$$\begin{aligned} p_1 &= p^n - \tau c_1 L_1(q^n, t^n), \\ q_1 &= q^n + \tau d_1 L_2(p_1), \\ \tau_1 &= t^n + \tau d_1. \end{aligned} \tag{21}$$

Second-stage:

$$\begin{aligned} p_2 &= p_1 - \tau c_2 L_1(q_{1,\tau_1}), \\ q_2 &= q_1 + \tau d_2 L_2(p_2), \\ \tau_2 &= \tau_1 + \tau d_2. \end{aligned} \tag{22}$$

Third-stage:

$$\begin{aligned} p_3 &= p_2 - \tau c_3 L_1(q_{2,\tau_2}), \\ q_3 &= q_2 + \tau d_3 L_2(p_3), \\ \tau_3 &= \tau_2 + \tau d_3. \end{aligned} \tag{23}$$

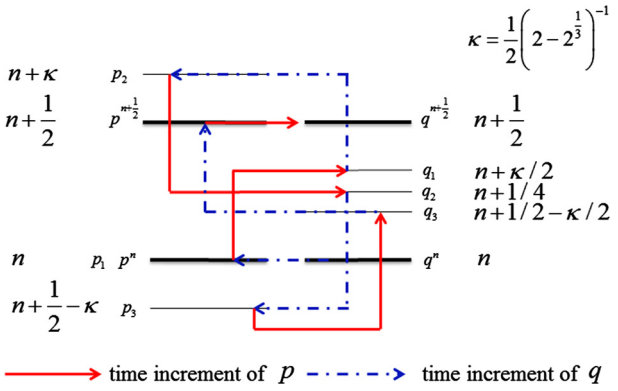

Fig. 1. Illustration of the 4-stage 4th-order explicit scheme applied between the two consecutive time steps n and $n+\frac{1}{2}$. Calculation of the solution starts from q^n to p_1 and, then, to q_1, p_2, q_2, p_3, q_3, $p^{n+\frac{1}{2}}$ and, finally, ends at $q^{n+\frac{1}{2}}$. (Note: The blue dash dot line, red solid line, black thin line and black bold line indicate the next time stage p. They are computed from the previous time-step solution of q, the next time-step solution q which is computed from the previous time-step solution of p, the temporary time stage and the updated time-step, respectively). (For interpretation of the references to color in this figure legend, the reader is referred to the web version of this article.)

Fourth-stage:

$$\begin{aligned} p^{n+\frac{1}{2}} &= p_3 - \tau c_4 L_1(q_{3,\tau_3}), \\ q^{n+\frac{1}{2}} &= q_3 + \tau d_4 L_2(p^{n+\frac{1}{2}}), \\ \tau^{n+\frac{1}{2}} &= \tau_3 + \tau d_4. \end{aligned} \tag{24}$$

In the above, τ is defined as $\frac{\Delta t}{2}$. Likewise, the functions $L_1(q,\tau_i)$ and $L_2(p)$ are expressed as $2q_{xx}$ and $2p_{xx}$, respectively, at the corresponding time stage. Advancement of the solutions p and q from $t^n = n\Delta t$ to the next time $t^{n+\frac{1}{2}} = (n+\frac{1}{2})\Delta t$ is illustrated in Fig. 1.

Based on the four-stage fourth-order accurate explicit symplectic PRK scheme given in equations (21)–(24), we can now easily derive the relations for $p^{n+\frac{1}{2}}$ from p^n and $q^{n+\frac{1}{2}}$ from q^n at two consecutive time steps. By substituting p^n into equation (21), then into equation (22), and finally into equation (24), we can get

$$\begin{aligned} p^{n+\frac{1}{2}} &= p^n - \Delta t q^n_{xx} - \frac{\Delta t^2}{2!} p^n_{xxxx} + \frac{\Delta t^3}{3!} q^{(6)} + \frac{\Delta t^4}{4!} p^{(8)} \\ &\quad + 0.09585\Delta t^5 q^{(10)} + 0.06475\Delta t^6 p^{(12)}, \\ q^{n+\frac{1}{2}} &= q^n + \Delta t p^n_{xx} - \frac{\Delta t^2}{2!} q^n_{xxxx} - \frac{\Delta t^3}{3!} p^{(6)} + \frac{\Delta t^4}{4!} q^{(8)} \\ &\quad - 0.09585\Delta t^5 p^{(10)} + 0.06475\Delta t^6 q^{(12)} + 0.04375\Delta t^7 p^{(14)}. \end{aligned} \tag{25}$$

Using the Taylor series expansion formula, or $f^{n+\frac{1}{2}} = f^n + f^n_t(\frac{\Delta t}{2}) + \frac{1}{2!} f^n_{tt}(\frac{\Delta t}{2})^2 + \frac{1}{3!} f^n_{ttt}(\frac{\Delta t}{2})^3 \ldots$, the following two modified equations can be derived

$$\begin{aligned} p_t + q_{xx} &= \Delta t^4 (0.09585 q^{(10)} - \frac{1}{2^5 5!} p^n_{ttttt}) \\ &\quad + \Delta t^5 (0.06475 p^{(12)} - \frac{1}{2^6 6!} p^n_{tttttt}) + O(\Delta t^6, \Delta x^4), \\ q_t - p_{xx} &= -\Delta t^4 (0.09585 p^{(10)} + \frac{1}{2^5 5!} q^n_{ttttt}) \\ &\quad + \Delta t^5 (0.06475 q^{(12)} - \frac{1}{2^6 6!} q^n_{tttttt}) + \Delta t^6 (0.04375 p^{(14)} - \frac{1}{2^7 7!} q^n_{ttttttt}) + O(\Delta t^7, \Delta x^4). \end{aligned} \tag{26}$$

Note that $p^{(n)}$ and $q^{(n)}$ denote the discrete expressions of $\frac{\partial^n p}{\partial x^n}|_{t=n\Delta t}$ and $\frac{\partial^n q}{\partial x^n}|_{t=n\Delta t}$, respectively. The scheme under investigation has therefore the temporal accuracy of order four.

3.1.2. DRE-preserving centered scheme for the linear Schrödinger equation

To minimize the numerical phase error while solving the linear Schrödinger equation (16), the idea of preserving dispersion relation equation (DRE), which was proposed firstly in the area of computational aeroacoustics by Tam and Webb [24], is adopted. One can refer to the work of Hairer [21] for other structure-preserving algorithms applied to solve the ordinary differential equation. In the current article, the spatial derivative term is approximated after applying the four-stage

fourth-order accurate explicit symplectic PRK temporal scheme for the linear part of the CNLS equation. To reduce the dispersive error generated normally from finite difference time domain (FDTD) methods, the difference between the exact and numerical dispersion relation equations for the linear Schrödinger equation is minimized.

By substituting the plane wave solution into the linear equation (16), the exact relation between the angular frequency ω and the wavenumber k is given by $\omega_{exact} = 2k^2$ or

$$\omega_{exact}\Delta t = 2(k\Delta x)^2\, Cr, \tag{27}$$

where $Cr = \frac{\Delta t}{\Delta x^2}$. To derive the numerical dispersion relation equation, the discrete plane wave solution is substituted into the nodal representations of ψ_j^n, $\psi_j^{n+\frac{1}{2}}$, $\psi_{j\pm m}^n$ to yield $\psi_j^n = \psi_j^n$, $\psi_j^{n+\frac{1}{2}} = e^{-\imath\omega\frac{\Delta t}{2}}\psi_j^n$ and $\psi_{j\pm m}^n = e^{\pm\imath mk\Delta x}\psi_j^n$. Development of the proposed scheme is followed by substituting them into the discrete equation

$$\imath\psi^{n+\frac{1}{2}} = \imath\psi^n - \Delta t\psi_{xx}^n - \imath\frac{\Delta t^2}{2!}\psi_{xxxx}^n + \frac{\Delta t^3}{3!}\psi^{(6)} + \imath\frac{\Delta t^4}{4!}\psi^{(8)} + 0.09585\Delta t^5\psi^{(10)} + \imath 0.06475\Delta t^6\psi^{(12)}, \tag{28}$$

which stems from the combination of equation (25) and the relationship (6). Note that $\psi^{(n)}$ denotes the discrete expression of $\frac{\partial^n\psi}{\partial x^n}|_{t=n\Delta t}$. The term $0.04375\Delta t^7 p^{(14)}$ will be truncated in this study. The numerical dispersion relation equation (DRE) for the linear Schrödinger equation can be derived as

$$\omega_{numerical}\Delta t = \arcsin(2\sin(\frac{\omega_{numerical}\Delta t}{2})\cos(\frac{\omega_{numerical}\Delta t}{2})), \tag{29}$$

where $\sin(\frac{\omega_{numerical}\Delta t}{2})$ and $\cos(\frac{\omega_{numerical}\Delta t}{2})$ result from the real and imaginary parts of equation (28), respectively. For the optimization of the numerical dispersion relation equation, we define the error function E as

$$\begin{aligned} E &= \sin^2(\frac{\omega_{exact}\Delta t}{2} - \frac{\omega_{numerical}\Delta t}{2}) \\ &= [\sin(\frac{\omega_{exact}\Delta t}{2})\cos(\frac{\omega_{numerical}\Delta t}{2}) - \cos(\frac{\omega_{exact}\Delta t}{2})\sin(\frac{\omega_{numerical}\Delta t}{2})]^2. \end{aligned} \tag{30}$$

The reason why we prefer the error function E defined in equation (30) is to make the integration of the equation $\int_{-m\pi}^{m\pi} E\, d(k\Delta x)$ possible. The error function E can now be minimized in an integral sense given below

$$\frac{\partial}{\partial\gamma}\int_{-m\pi}^{m\pi} E\, d(k\Delta x) = 0. \tag{31}$$

The value of m is in the range between 0 and 1.

Since equation (31), which involves unknowns m and γ, is not amenable to analytical integration, we resort to the numerical approach by changing the value of m in the range between 0 and 1. Through a series of computational exercises, the optimal value of γ ($\equiv -0.08336826007$), which is now the only unknown in (20), is obtained at $m = 0.104329$. It is worthy to note here that the numerically determined values for m and γ render the minimal value of E defined in (30). Having obtained the optimal value of γ, the derived numerical dispersion relation equation gives us the relation between the numerical angular frequency $\omega_{numerical}\Delta t$ and the modified wavenumber $k\Delta x$. The derived expression of dispersion relation equation is very complex and we only plot $\omega_{numerical}\Delta t$ versus the modified wavenumber $k\Delta x$ in Fig. 2.

The phase velocity v_p describes the speed at which the phase of a wave propagates in the direction normal to the propagating waveform. It is therefore worthy to plot the physically meaningful velocity with respect to the modified wavenumber $k\Delta x$ in Fig. 3. As the value of $k\Delta x$ becomes smaller than 1.35, good match between the numerical and exact dispersion relation equations can be clearly seen.

Since the FDTD method developed in this study is explicit, Von Neumann (or Fourier) stability analysis needs to be performed on the system of four-stage fourth-order accurate explicit symplectic PRK equations. Here the condition $|G| \le 1$, where $|G|$ is the amplification factor, is enforced to ensure that numerical stability condition is deemed satisfied. In Fig. 4, it can be easily seen that $|G| \le 1$ when the value Cr ($\equiv \frac{\Delta t}{\Delta x^2}$) is smaller than 0.25. For completeness, one can refer to Appendix A for the detailed stability analysis.

3.2. Numerical method for nonlinear part of Schrödinger equation

Since $|\psi|^2$ is equal to $\psi\overline{\psi}$, one can get

$$\partial_t|\psi|^2 = \psi_t\overline{\psi} + \psi\overline{\psi}_t. \tag{32}$$

According to the nonlinear equation (17), the term ψ_t is substituted into equation (32) to yield the following equation

$$\frac{\partial|\psi|^2}{\partial t} = 0. \tag{33}$$

The value of $|\psi|^2$ is therefore invariant with time.

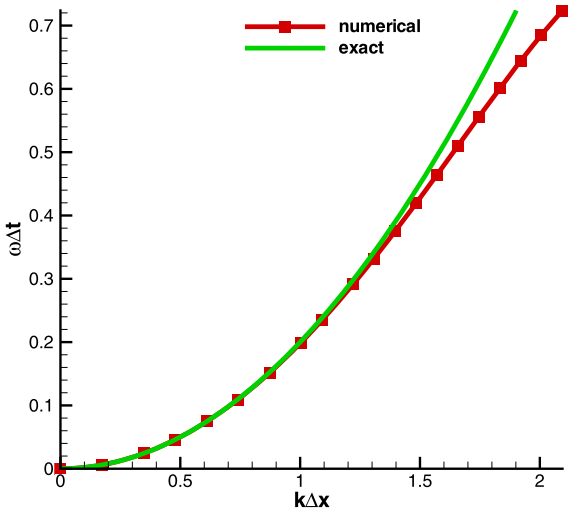

Fig. 2. Comparison of the derived numerical and exact angular frequencies $\omega\Delta t$, which are plotted with respect to the modified wavenumber $k\Delta x$.

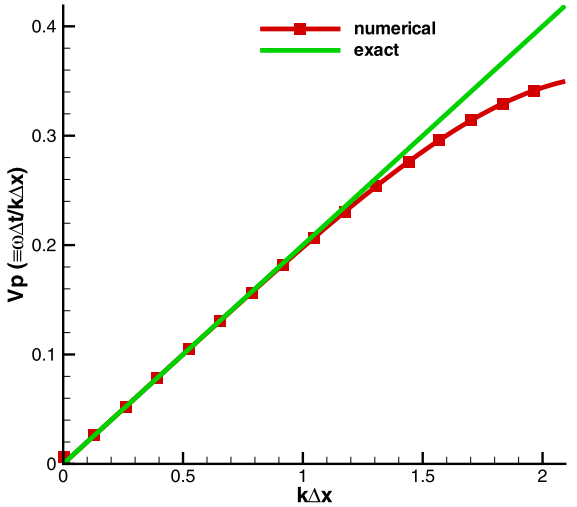

Fig. 3. Comparison of the numerical and exact phase velocities v_p ($\equiv \frac{\omega\Delta t}{k\Delta x}$), which are plotted with respect to the modified wavenumber $k\Delta x$, using the proposed scheme.

Thanks to the existing invariant nature of $|\psi|^2$ within each time increment while employing the linear–nonlinear temporal splitting method, the solution of the nonlinear ordinary differential equation (17) can be derived analytically as $\psi = e^{i4|\psi|^2 t}$. The discretized representation of this equation is $\psi^{n+1} = \psi^{n+\frac{1}{2}} e^{i2|\psi|^2\Delta t}$. The resulting expressions for p and q turn out to be $p^{n+1} = p^{n+\frac{1}{2}}\cos(2|\psi|^2\Delta t) - q^{n+\frac{1}{2}}\sin(2|\psi|^2\Delta t)$ and $q^{n+1} = p^{n+\frac{1}{2}}\sin(2|\psi|^2\Delta t) + q^{n+\frac{1}{2}}\cos(2|\psi|^2\Delta t)$, where $|\psi|^2$ is equal to $(p^{n+\frac{1}{2}})^2 + (q^{n+\frac{1}{2}})^2$ at the time step $n+\frac{1}{2}$.

4. 2D cubic nonlinear Schrödinger equation solver

In this section we intend to solve the following NLS equation in (x, y) plane

$$\imath\psi_t + \psi_{xx} + \psi_{yy} + \beta|\psi|^2\psi = 0. \tag{34}$$

The linear–nonlinear splitting strategy described in Section 3 for solving the one-dimensional equation can be applied as well to compute the solution of the above two-dimensional CNLS equation. This splitting of equation (34) leads to the respective linear and nonlinear equations given below

$$\imath\psi_t + 2\psi_{xx} + 2\psi_{yy} = 0, \tag{35}$$

$$\imath\psi_t + 2\beta|\psi|^2\psi = 0. \tag{36}$$

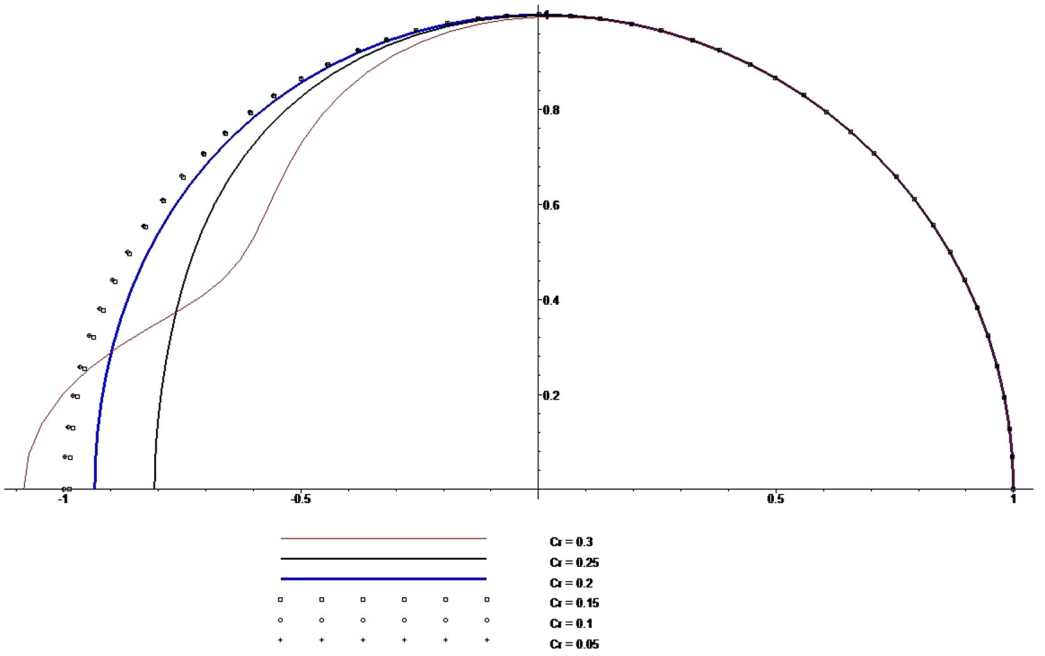

Fig. 4. The magnitudes of the amplification factors, or $|G|$, are plotted with respect to the modified wavenumber at different values of Cr ($\equiv Cr_x = \frac{\Delta t}{\Delta x^2}$) for the proposed one-dimensional scheme.

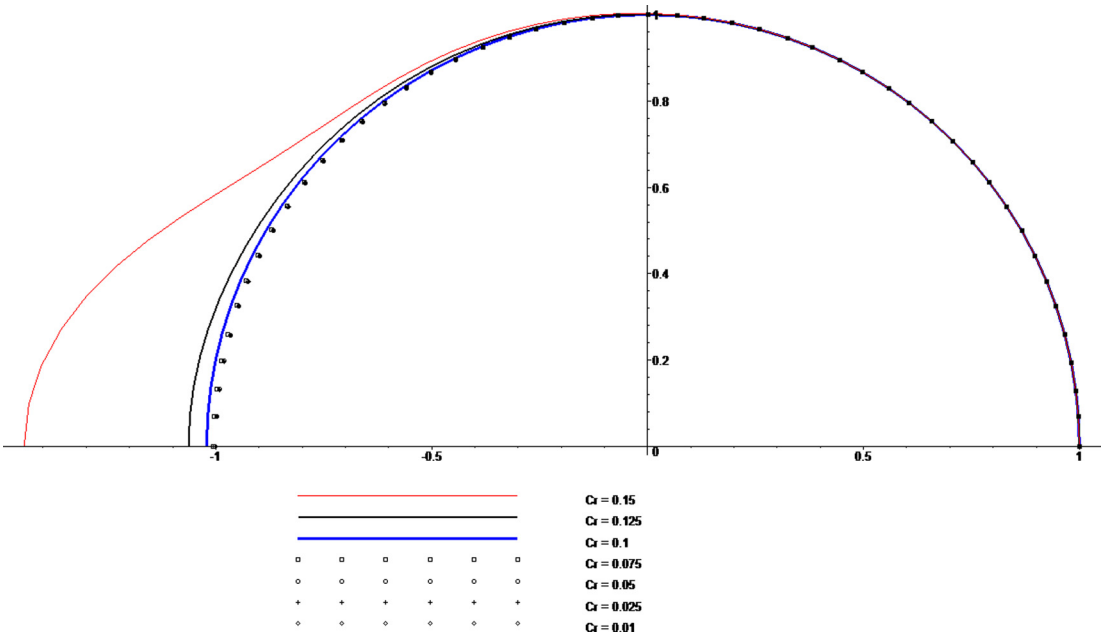

Fig. 5. The magnitudes of the amplification factor, or $|G|$, are plotted with respect to the modified wavenumber at different values of Cr ($\equiv Cr_x = \frac{\Delta t}{(\Delta x)^2}$) for the proposed two-dimensional scheme developed under $\Delta x = \Delta y$.

Explicit symplecticity- and dispersion-relation-equation-preserving scheme can be directly developed from the two-dimensional linear equation (35). One can see clearly from Fig. 5 that a direct calculation of the two-dimensional equation suffers a comparatively stringent stability condition imposed on the adopted explicit scheme. The details of the two dimensional stability analysis can be also seen in Appendix A.

To alleviate the problem of stability condition described above when applying the proposed explicit scheme to solve the two-dimensional equation (34), the method of fractional steps or the method of splitting is adopted in this study. The basic

Table 1
Comparison of the L_2-*error norms* for the real part (top) and the imaginary part (bottom) of the complex-valued wavefunction ψ, which are computed at different grid spacings using (a) Crank–Nicolson scheme [27]; (b) linearized Crank–Nicolson scheme I [27]; (c) linearized Crank–Nicolson scheme II [27]; (d) three-level explicit scheme [27]; (e) Hopscotch scheme [27]; (f) Hopscotch scheme with extrapolation [27]; (g) splitting-spectral scheme [27]; (h) present scheme, respectively.

L_2-error norms of $\Re(\psi) \equiv p$						
n	1	2	4	8	16	Rate of convergence (spatial)
(a)	3.32E−02	8.16E−03	2.09E−03	5.07E−04	1.27E−04	2.0069
(b)	3.47E−02	8.17E−03	2.03E−03	5.07E−04	1.27E−04	2.0198
(c)	3.43E−02	8.16E−03	2.03E−03	5.07E−04	1.27E−04	2.0167
(d)	3.34E−02	8.10E−03	2.03E−03	5.07E−04	1.27E−04	2.0077
(e)	8.77E−03	2.25E−03	5.70E−04	1.44E−04	5.72E−05	1.8482
(f)	4.94E−02	1.26E−02	3.16E−03	7.75E−04	2.13E−04	1.9738
(g)	1.79E−04	1.66E−04	1.60E−04	1.57E−04	1.55E−04	0.0482
(h)	1.48E−03	2.95E−04	7.76E−05	1.98E−05	4.98E−06	2.0327
L_2-error norms of $\Im(\psi) \equiv q$						
n	1	2	4	8	16	Rate of convergence (spatial)
(a)	3.43E−02	8.40E−03	2.03E−03	5.22E−04	1.30E−04	2.0089
(b)	3.25E−02	8.42E−03	2.09E−03	5.22E−04	1.30E−04	2.0022
(c)	3.32E−02	8.40E−03	2.09E−03	5.22E−04	1.30E−04	1.9990
(d)	3.23E−02	8.34E−03	2.08E−03	5.21E−04	1.30E−04	1.9903
(e)	8.26E−03	2.09E−03	5.28E−04	1.34E−04	6.52E−05	1.7927
(f)	5.13E−02	1.30E−02	3.25E−03	7.97E−04	2.14E−04	1.9833
(g)	2.47E−04	2.41E−04	2.38E−04	2.36E−04	2.35E−04	0.0171
(h)	1.44E−03	3.13E−04	8.45E−05	2.16E−05	5.45E−06	1.9949

idea of our adopted method to resolve the stability problem is to split the two-dimensional equation into the following set of one-dimensional linear equations

$$\imath\psi_t + \psi_{xx} = 0, \tag{37}$$

$$\imath\psi_t + \psi_{yy} = 0. \tag{38}$$

The operator splitting of equation (34) makes it possible to advance the calculation of Schrödinger solution in x- and y-directions subject to their respective maximum allowable time steps. This fractional step method has a close relation to the alternating direction implicit (ADI) method that was developed at about the same time. Use of this splitting method renders a compelling advantage over a non-splitting method provided that the allowable time increments Δt_x and Δt_y are much different from those using the currently employed explicit scheme because of the large difference in the grid spacings. The reader is urged to consult the book of Yanenko [25].

Now we will make use of the explicit FDTD scheme developed in Section 3.1 to solve the one-dimensional linear Schrödinger equation. Application of the three-term splitting method in [26] yields the following equations for p and q, where $\psi = p + \imath q$.

$$\imath\psi_t + 3\psi_{xx} = 0, \tag{39}$$

$$\imath\psi_t + 3\psi_{yy} = 0, \tag{40}$$

$$\imath\psi_t + 3\beta|\psi|^2\psi = 0. \tag{41}$$

Our implementation of the time marching scheme to get the two-dimensional Schrödinger solution from t^n to t^{n+1} is described below. In the first fractional step of calculating the solution from $t^n = n\Delta t$ to $t_1 = (n + \frac{1}{9})\Delta t$, we perform firstly the calculation of equation (41) and then from t_1 to $t_2 = (n + \frac{4}{9})\Delta t$ on (39). This is followed by calculating the solution from equation (41) from t_2 to $t_3 = (n + \frac{5}{9})\Delta t$ and then from t_3 to $t_4 = (n + \frac{8}{9})\Delta t$ on (40), and finally from t_4 to $t^{n+1} = (n + 1)\Delta t$ on (41).

In view of the above three split equations, the explicit symplecticity- and dispersion-relation-equation-preserving scheme developed for the one-dimensional NLS equation can now be readily applied to solve the two-dimensional NLS equation.

5. Verification study

The proposed symplecticity- and dispersion-relation-equation-preserving scheme is verified by solving the problems amenable to exact solutions. Both one- and two-dimensional NLS equations are considered in this section. Furthermore, the present scheme is applied to simulate the solution under the computationally challenging semiclassical limit.

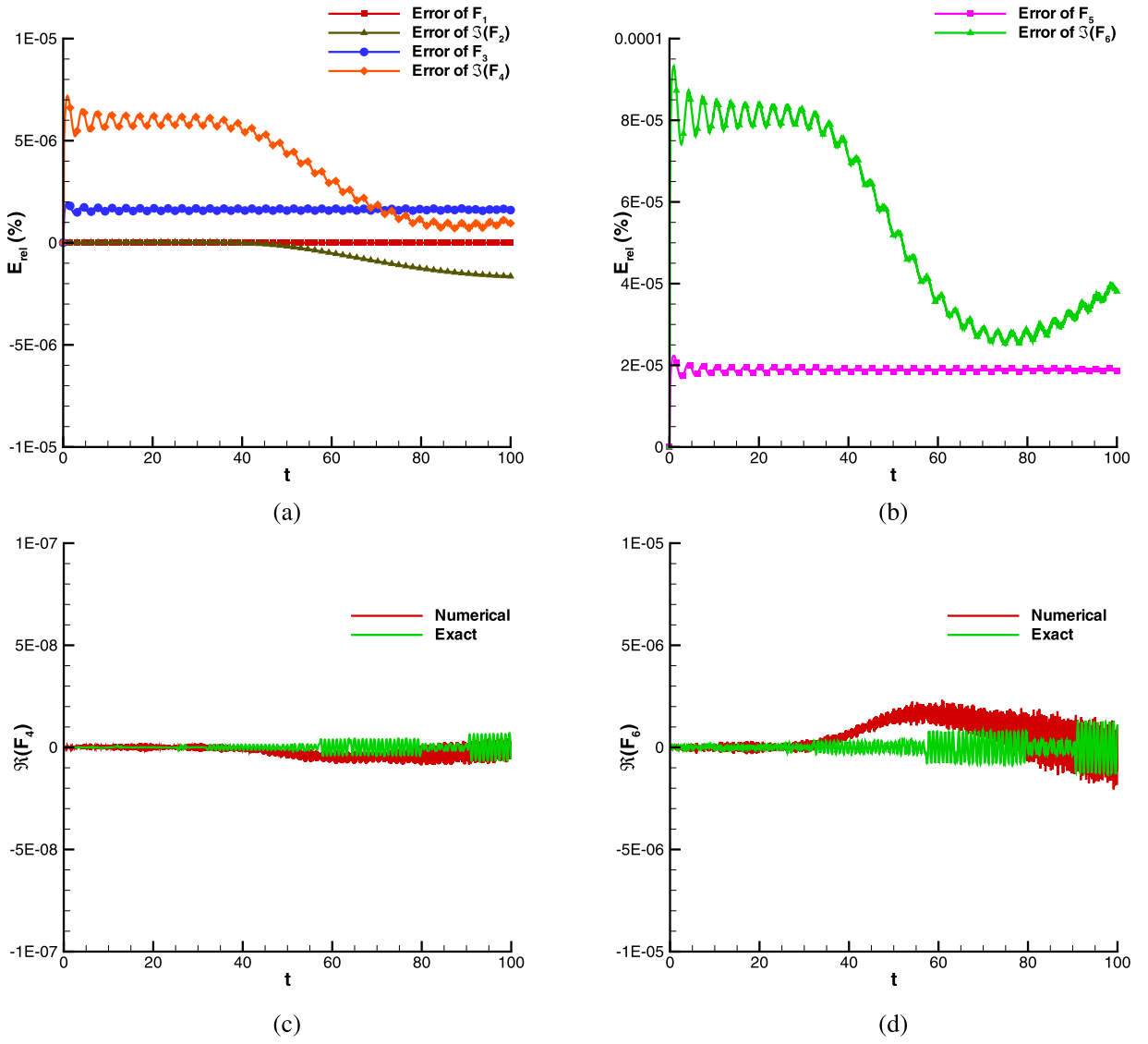

Fig. 6. Comparison of the relative error percentages ($E_{rel,i} \equiv \frac{E_{numerical,i} - E_{exact,i}}{E_{exact,i}} \times 100\%$) ($i = 1 - 6$) between the exact and predicted Hamiltonian values for $F_1(t)$, $\Im(F_2(t))$, $F_3(t)$, $\Im(F_4(t))$ in (a) and $F_5(t)$, $\Im(F_6(t))$ in (b). Comparison of the exact and predicted values of the Hamiltonians $\Re(F_4(t))$ in (c) and $\Re(F_6(t))$ in (d) computed at $Cr = 0.25$ and $\Delta x = 0.025$, where $\Re$ and $\Im$ denote the real and imaginary parts, respectively.

5.1. One-dimensional analytical problem

We start by solving the CNSE equation (4), which is amenable to the following exact solution, in the domain of $-8 \leq x \leq 8$ [6]

$$\psi_{exact}(x,t) = sech(\frac{\sqrt{\varepsilon}x + 4t}{\varepsilon}) \exp(\frac{-2\imath}{\varepsilon}(\sqrt{\varepsilon}x + \frac{3}{2}t))/\sqrt{\varepsilon}. \tag{42}$$

Subject to the initial condition $\psi(x,0) = sech(\frac{x}{\sqrt{\varepsilon}}) \exp(\frac{-2\imath}{\sqrt{\varepsilon}}x)/\sqrt{\varepsilon}$, the solution of (4) is sought at $\varepsilon = 0.5$ and Cr $(\equiv \Delta t/(\Delta x)^2) = 0.25$.

For the verification and comparison purposes, the L_2-*norm* errors at $t = 0.5$ are obtained firstly from a series of calculations performed at the continuously refined meshes $\Delta x = 1/8n$ $(n = 1, 2, 4, 8, 16)$ for the real part ($\Re(\psi)$ or p) and the imaginary part ($\Im(\psi)$ or q) of the complex wavefunction ψ, respectively. According to the computed results in Table 1 for the real (top) and imaginary (bottom) parts, respectively, the proposed scheme is verified to be applicable to solve NLS equation. The corresponding rates of convergence are also tabulated in Table 1. One can clearly see that the currently predicted

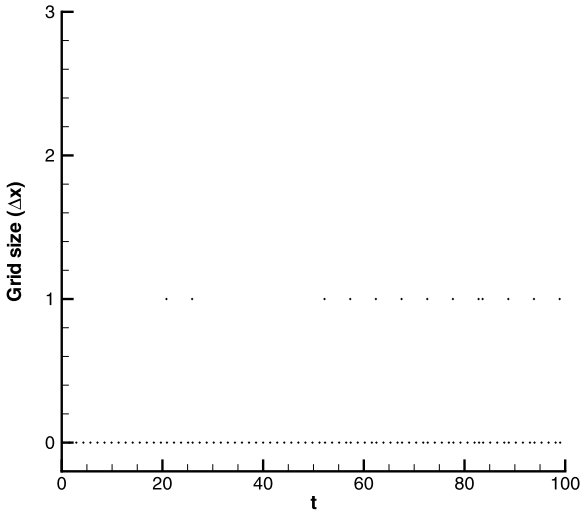

Fig. 7. The difference of the predicted and exact nodal crest locations x_i $(i = 1 - N)$ is plotted with respect to time computed at $Cr = 0.25$ and $\Delta x = 0.025$.

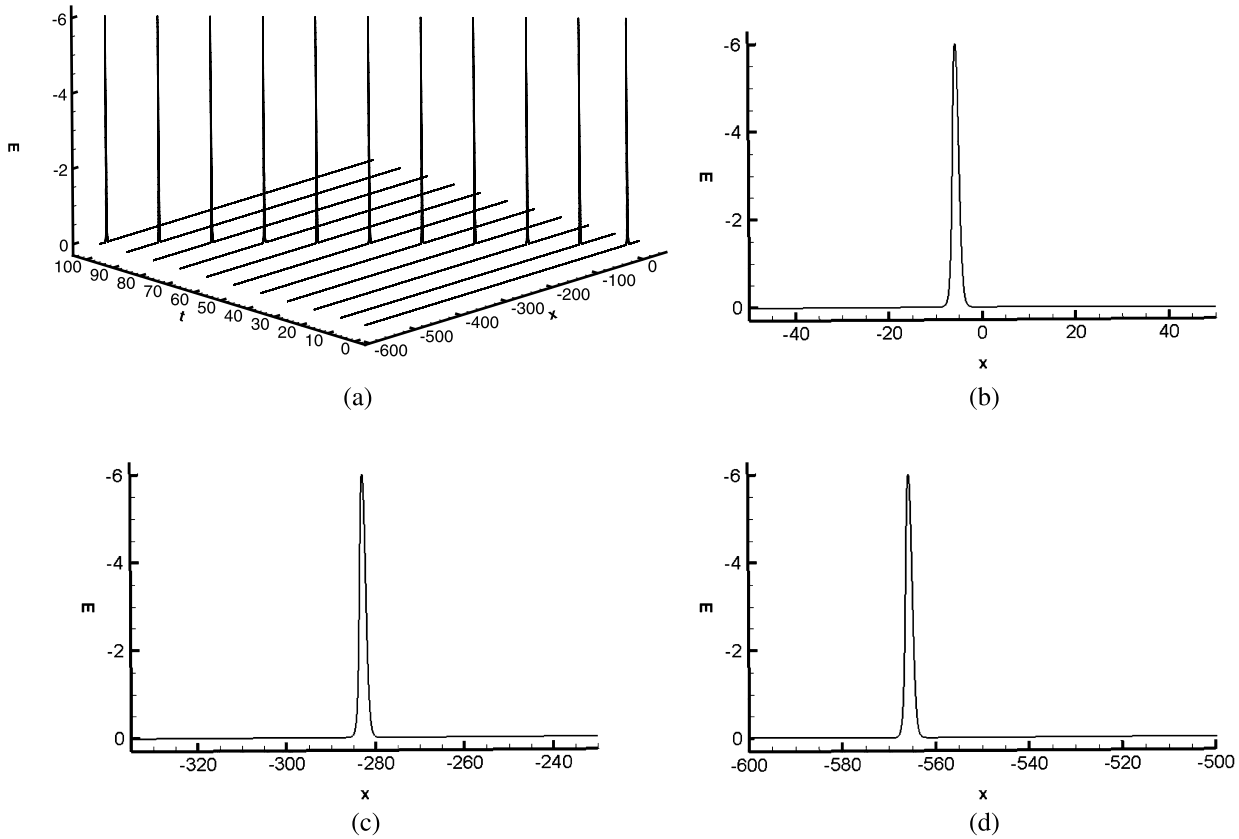

Fig. 8. (a) The predicted values of energy E $(\equiv \frac{1}{2}[(p^2+q^2)^2 - (v^2+w^2)])$ are plotted with respect to time and space. (b), (c), (d) are the zoomed views of E at $t = 1, 50, 100$, respectively.

solution accuracy is better than the other finite difference schemes listed in [27]. The rates of convergence tabulated also in Table 1 for p $(\equiv \Re(\psi))$ and q $(\equiv \Im(\psi))$ using the current finite difference scheme, which can preserve both symplecticity and dispersion relation equation, are much larger than those computed by other methods.

To demonstrate that the proposed scheme is indeed symplectic, the Hamiltonians expressed in equations (10)–(15) are calculated and are plotted with respect to time. In Figs. 6(a)–6(d), all the Hamiltonians are perfectly conserved numerically

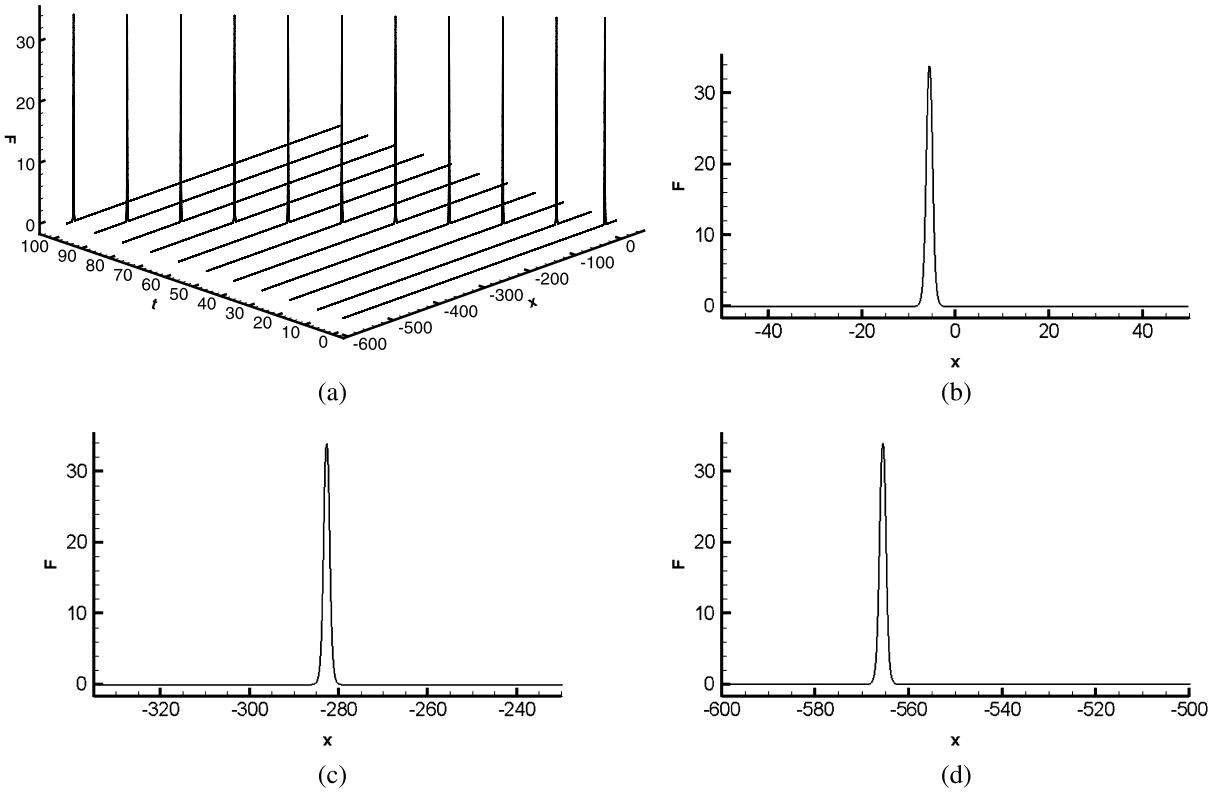

Fig. 9. (a) The predicted values of energy F ($\equiv wp_t + vq_t$) are plotted with respect to time and space. (b), (c), (d) are the zoomed views of F at $t = 1, 50, 100$, respectively.

at $Cr = 0.25$ and $\Delta x = 0.025$ in the computational domain $x \in [-50, 600]$ and $t \in [0, 100]$. To confirm the fact that the proposed scheme can be applied to obtain a wave solution with very accurately predicted phase speed, the discrepancy between the exact and the numerically predicted nodal crest locations is plotted in Fig. 7 with respect to time. In Fig. 7, the largest discrepancy between the exact and numerical nodal crest locations is one Δx.

To provide some propagation details of the Schrödinger equation, the energy E ($\equiv \frac{1}{2}[(p^2+q^2)^2 - (v^2+w^2)]$), energy flux F ($\equiv wp_t + vq_t$), momentum I ($\equiv \frac{1}{2}(pv - qw)$), momentum flux G ($\equiv [v^2 + w^2 + \frac{1}{2}(p^2+q^2)^2] - \frac{1}{2}(pq_t - qp_t)$), $N = \frac{1}{2}(p^2+q^2)$ and $M = pq_x - qp_x$ are plotted in Figs. 8–13, respectively, based on the computed values of p, q, v and w. Having calculated the values of E, F, I, G, N and M for $t \in [0, 100]$, three equations $\frac{\partial E}{\partial t} + \frac{\partial F}{\partial x} = 0$, $\frac{\partial I}{\partial t} + \frac{\partial G}{\partial x} = 0$ and $\frac{\partial N}{\partial t} + \frac{\partial M}{\partial x} = 0$ have been numerically verified to be correct according to the plots shown in Fig. 14. The proposed scheme is proved again to be applicable to simulate the CNLS equation.

Calculation of the cubic nonlinear Schrödinger solution at the so-called semiclassical limit has been known to be computationally challenging [9]. For this reason, the proposed numerical method is applied to solve the Schrödinger equation (3) cast in the semiclassical scale. Our purpose is to compare the simulated solutions with other solutions presented in the works of [9,10,28] for the sake of validation. In this study, the classical Wentzel–Kramers–Brillouin (WKB) (or known as Liouville–Green) form is chosen as our initial condition $u(x,0) = \sqrt{n_0(x)}e^{\imath S_0(x)/\varepsilon}$, where $n_0(x) = (e^{-25(x-0.5)^2})^2$ decays considerably fast when $|x|$ approaches to infinity. In this validation study, we consider $S_0(x) = -\frac{1}{5}\ln(2\cosh(5(x-0.5)))$ and $V(x) = -10$ in the domain of $0 \le x \le 1$. As ε approaches zero, this investigated problem permits theoretically weak solution [10]. For the linear potential case considered in [9,10,28], the predicted results at $\varepsilon = 0.0064, 0.0001$, $\Delta x = 0.01, 0.0001$ and $\Delta t = 0.0001, 5.0\text{E}{-6}$ are shown in Fig. 15 for the physical quantity $\rho(x,t)$ ($\equiv |u(x,t)|^2$) and for the current density $J(x,t)$ ($\equiv \frac{\varepsilon}{2\imath}(\bar{u}\nabla u - u\nabla\bar{u})$), respectively. At $t = 0.54$, our predicted results agree well with the results of Markowich et al. [10] obtained at the weak limit or under the condition when the value of ε is closed to zero.

As far as the nonlinear potential $V(x,|u|^2) = -|u|^2$ is considered, the defocusing solution exhibits ε-oscillation behavior. The initial condition is considered as $u(x, t=0) = A(x)e^{\imath S_0(x)/\varepsilon}$, where $A(x) = e^{-x^2}$ and $S_0(x) = -\frac{1}{5}\ln(2\cosh(5x))$ in the domain of $[-4, 4]$. For the cases investigated at $\varepsilon = 0.01, 0.0025$, $\Delta x = 0.005, 0.001$ and $\Delta t = 0.001, 0.0001$, the predicted results plotted in Fig. 16 are all compared well with the results given in [9,28–30] for $\rho(x,t)$ ($\equiv |u(x,t)|^2$) and $J(x,t)$ ($\equiv \frac{\varepsilon}{2\imath}(\bar{u}\nabla u - u\nabla\bar{u})$), respectively, at $t = 1$. Our aim of showing that we can accurately predict Schrödinger solution at a very small value of ε is achieved.

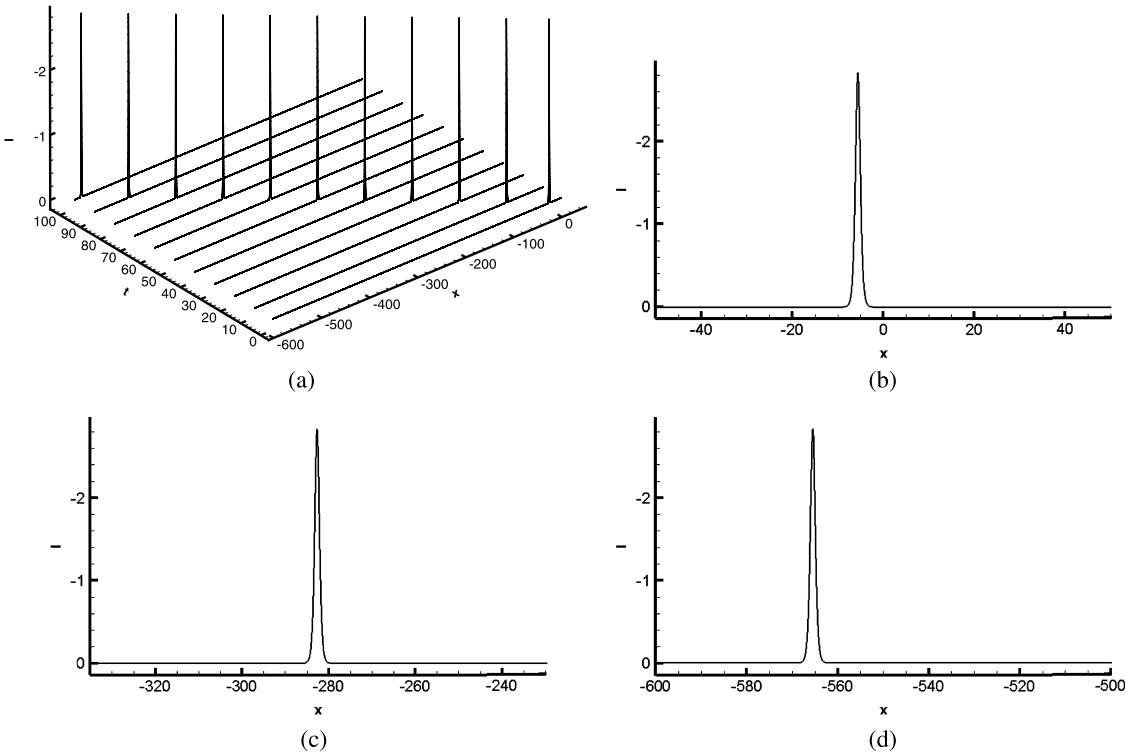

Fig. 10. (a) The predicted values of energy I ($\equiv \frac{1}{2}(pv - qw)$) are plotted with respect to time and space. (b), (c), (d) are the zoomed views of I at $t = 1, 50, 100$, respectively.

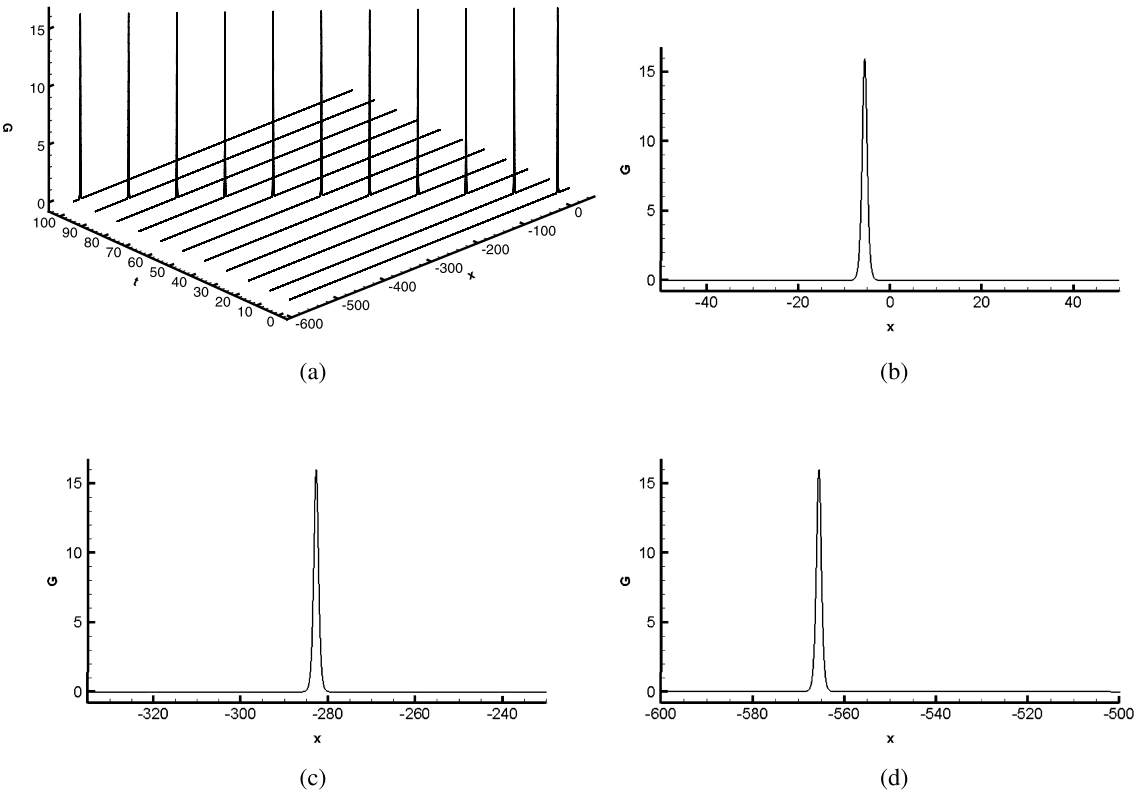

Fig. 11. (a) The predicted values of energy G ($\equiv [v^2 + w^2 + \frac{1}{2}(p^2 + q^2)^2] - \frac{1}{2}(pq_t - qp_t)$) are plotted with respect to time and space. (b), (c), (d) are the zoomed views of G at $t = 1, 50, 100$, respectively.

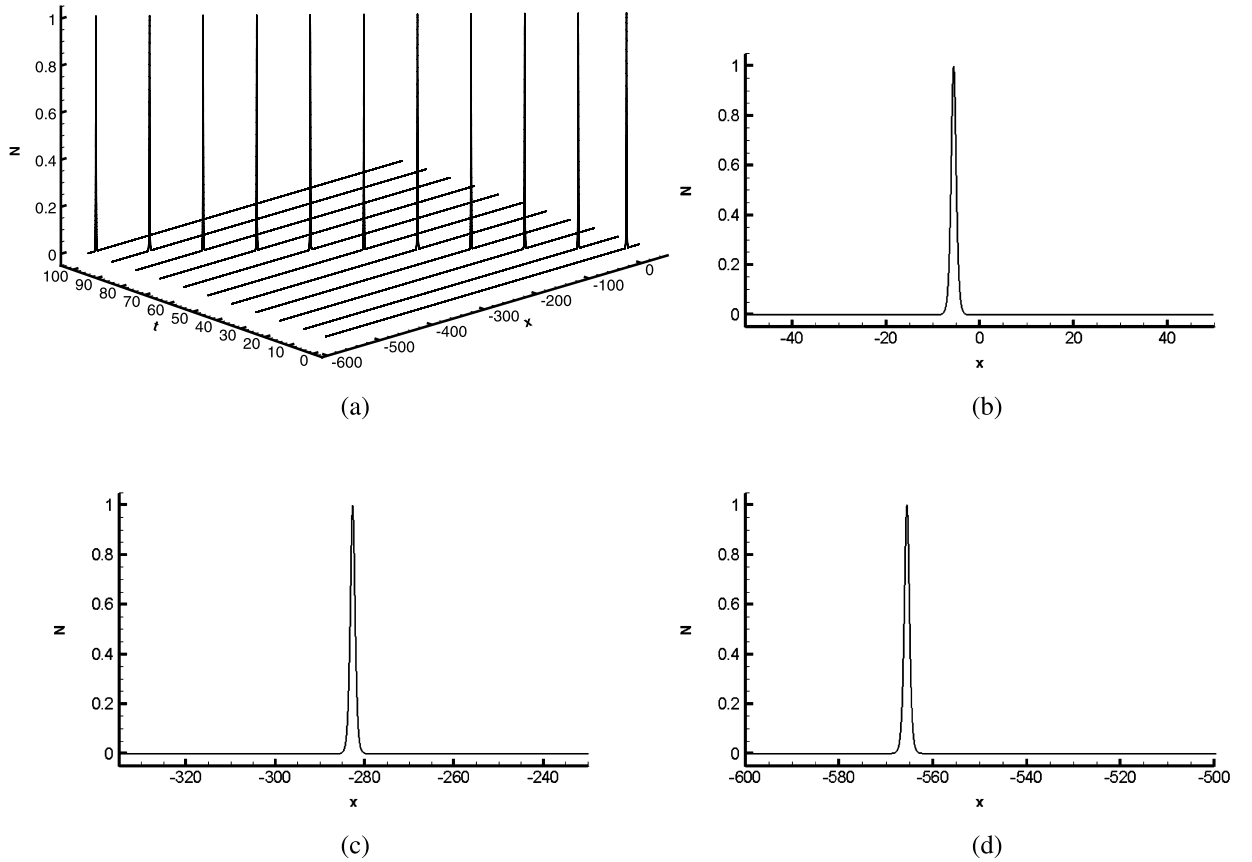

Fig. 12. (a) The predicted values of energy N ($\equiv \frac{1}{2}(p^2+q^2)$) are plotted with respect to time and space. (b), (c), (d) are the zoomed views of N at $t = 1, 50, 100$, respectively.

5.2. Two-dimensional Schrödinger equation with exact solution

The three-term splitting method applied to solve the two-dimensional NLS equation is then verified by solving equation (34) in a square $[0, 2\pi] \times [0, 2\pi]$. Subject to the Dirichlet boundary condition prescribed at the domain boundary, the simulated solutions at $t = 1$ under $\Delta t = 10^{-4}$ and $\Delta x = \Delta y = \frac{2\pi}{N}$, where $N = 10, 20, 40, 80$, will be compared with the corresponding exact solutions given below for $\beta = 2$

$$\psi_{exact}(x, y, t) = e^{\iota[x+y-(2-\beta)t]}. \tag{43}$$

In Table 2, we have tabulated the predicted L_2 and L^∞ error norms. Excellent agreement between the exact and simulated solutions confirms the legitimacy of applying the method of fractional steps in the calculation of solution from the two-dimensional Schrödinger equation. For a further verification of the proposed solver for the NLS equation in two dimensions, the following three conserved quantities are calculated and are then plotted with respect to time [26]

$$\int \frac{1}{2}(q\bar{u} - pg)\, d\Omega = C_1, \tag{44}$$

$$\int \frac{1}{2}(p\bar{v} - pw)\, d\Omega = C_2, \tag{45}$$

$$\int -\frac{1}{2}(p^2+q^2)^2 + \frac{1}{2}(\bar{u}^2 + \bar{v}^2 + g^2 + w^2)\, d\Omega = -C_3, \tag{46}$$

where $\bar{u}$, $\bar{v}$, g and w denote p_x, p_y, q_x and q_y, respectively. In the above, the integrands in (44) and (45) denote the momentum densities. According to Fig. 17, these conservation laws embedded in the two-dimensional NLS equation (34) are deemed satisfied discretely.

For completeness, the energy density E, energy fluxes F_1, F_2, momentum densities I_1, I_2, and momentum fluxes G_{ij} $(i, j = 1, 2)$ defined below are also calculated from the computed solution

$$E = -\frac{\beta}{4}(p^2+q^2)^2 + \frac{1}{2}(\bar{u}^2 + \bar{v}^2 + g^2 + w^2), \tag{47a}$$

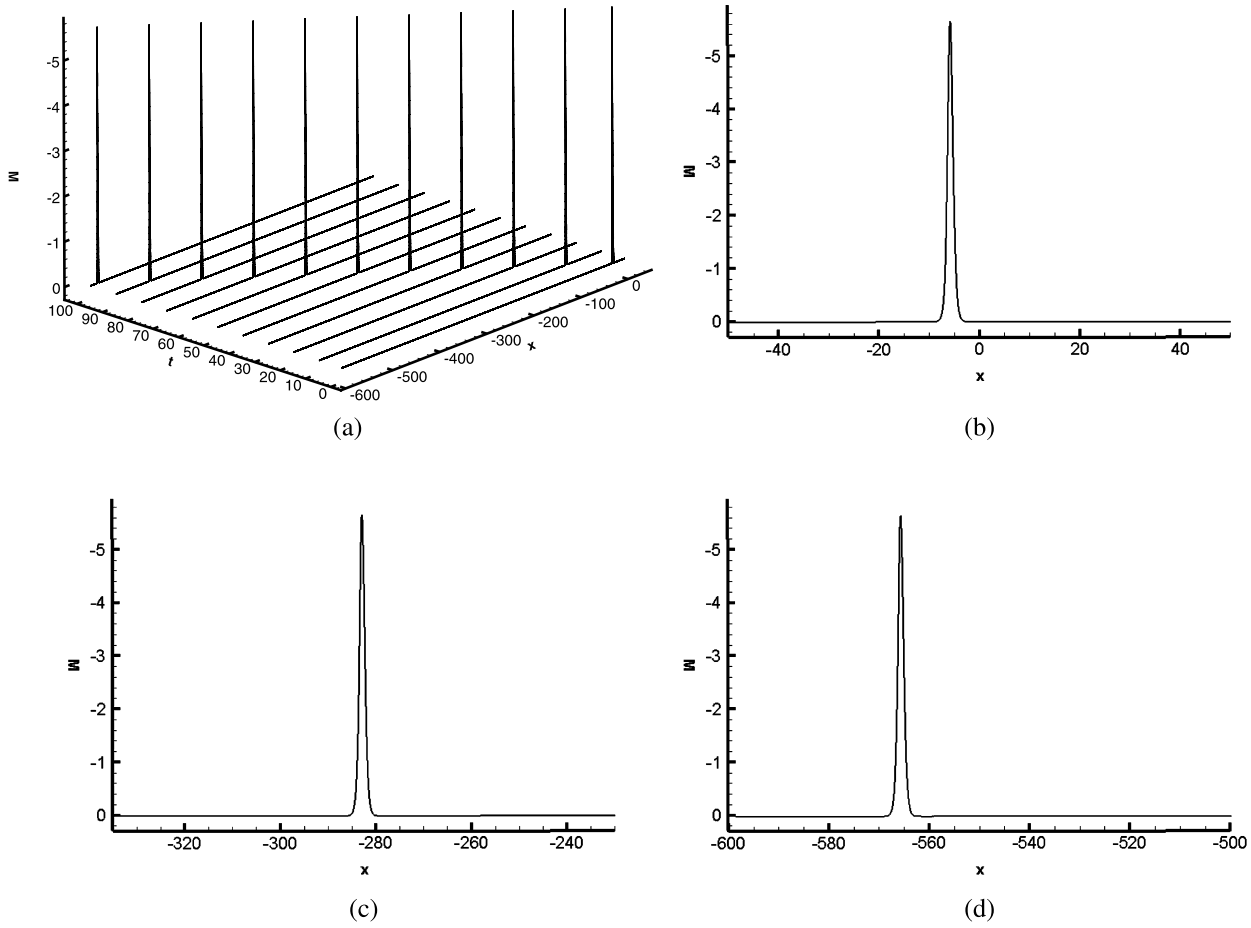

Fig. 13. (a) The predicted values of energy M ($\equiv pq_x - qp_x$) are plotted with respect to time and space. (b), (c), (d) are the zoomed views of M at $t = 1, 50, 100$, respectively.

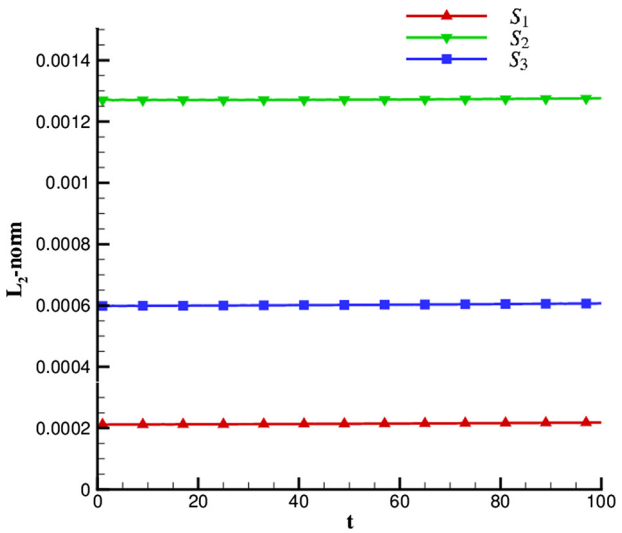

Fig. 14. The computed L_2-*norms* of S_1, S_2 and S_3 defined as $\frac{\partial N}{\partial t} + \frac{\partial M}{\partial x} = S_1$, $\frac{\partial E}{\partial t} + \frac{\partial F}{\partial x} = S_2$ and $\frac{\partial I}{\partial t} + \frac{\partial G}{\partial x} = S_3$, respectively, are plotted with respect to time at $\Delta t = 0.0005$ and $\Delta x = 0.05$ for $t \in [0, 100]$ and $x, y \in [-600, 50]$.

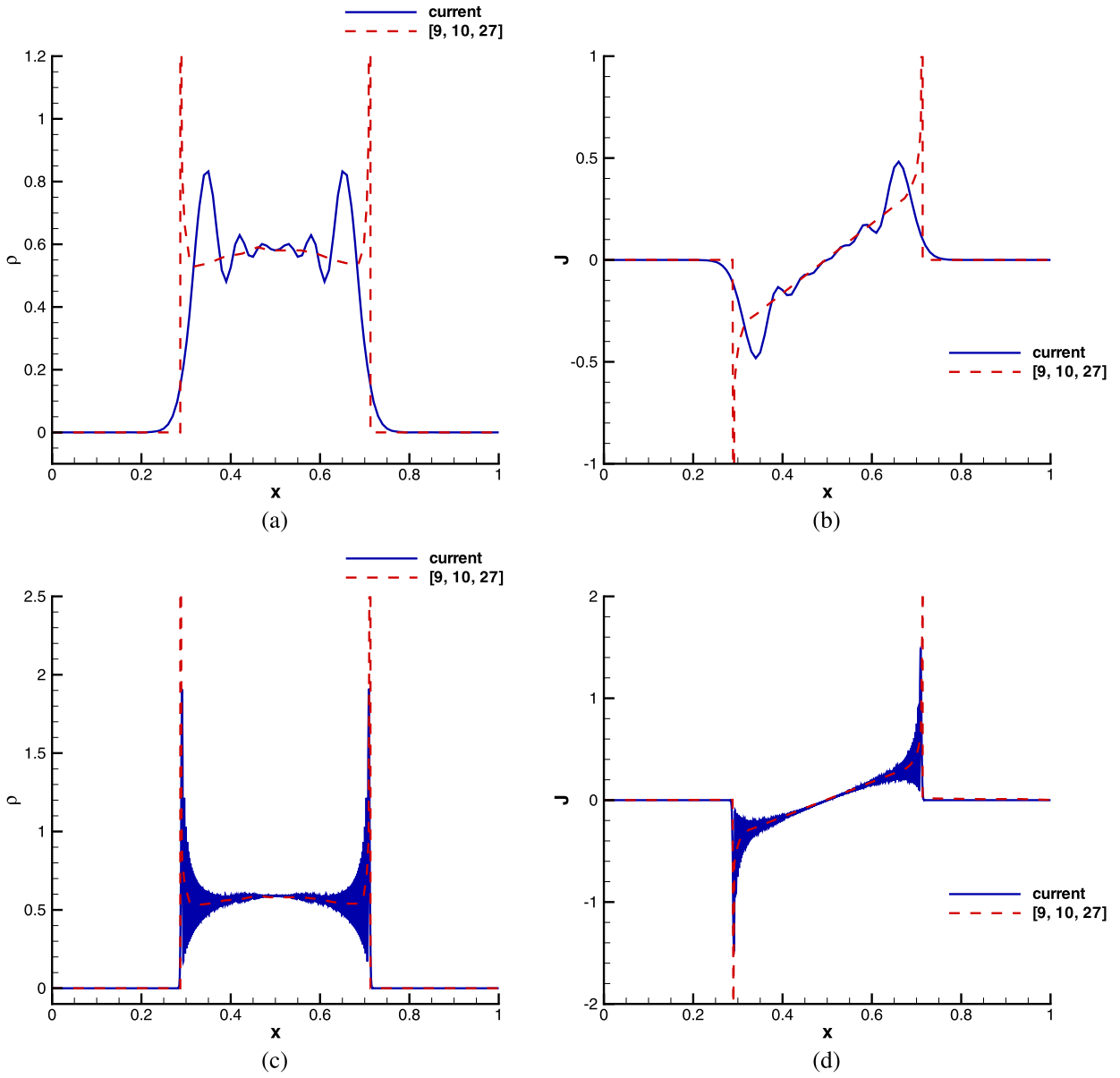

Fig. 15. Comparison of numerical and weak limit results in (a) and (b), at $t = 0.54$ for ρ and J computed at $\varepsilon = 0.0064$, $\Delta x = 0.01$ and $\Delta t = 0.0001$, respectively. Comparison of numerical and weak limit results in (c) and (d) at $t = 0.54$ for ρ and J computed at $\varepsilon = 0.0001$, $\Delta x = 0.00005$ and $\Delta t = 2.5\text{E}{-6}$, respectively.

$$F_1 = -\bar{u}p_t - gq_t, \tag{47b}$$

$$F_2 = -\bar{v}p_t - wq_t, \tag{47c}$$

$$I_1 = \frac{1}{2}(q\bar{u} - pg), \tag{47d}$$

$$I_2 = \frac{1}{2}(p\bar{v} - pw), \tag{47e}$$

$$G_{11} = -\frac{\beta}{4}(p^2+q^2)^2 - \frac{1}{2}(\bar{u}^2+g^2) - \frac{1}{2}(qp_t - pq_t) - \frac{1}{2}(p\bar{v}_y + qw_y), \tag{47f}$$

$$G_{12} = \frac{1}{2}(-\bar{u}\bar{v} - gw + p\bar{v}_x + qw_x), \tag{47g}$$

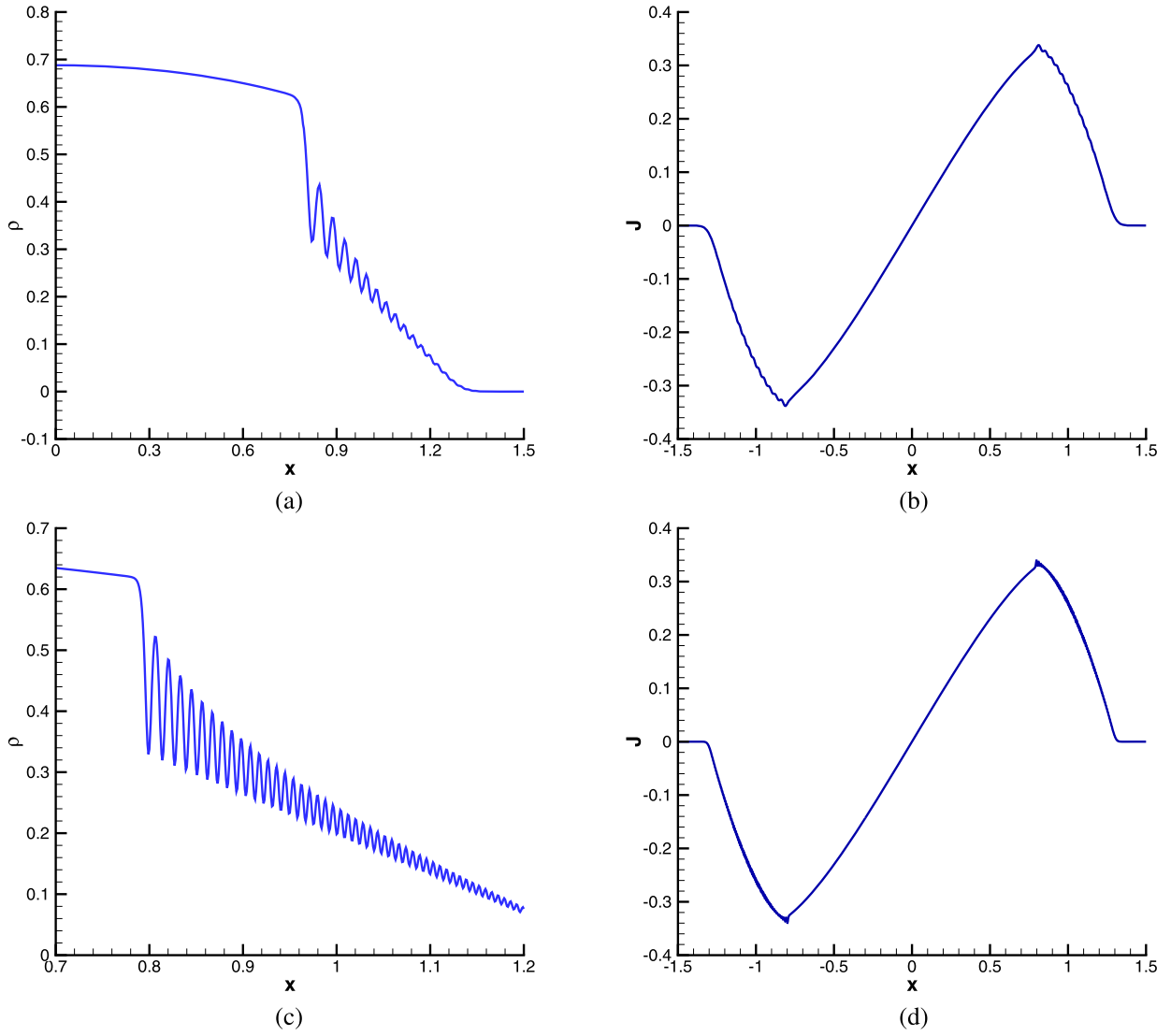

Fig. 16. The predicted results of ρ and J at $t = 1$ for the simulation carried out at $\varepsilon = 0.01$, $\Delta x = 0.005$ and $\Delta t = 0.001$ in (a), (b), respectively. The numerical results of ρ and J at $t = 1$ for the simulation carried out at $\varepsilon = 0.0025$, $\Delta x = 0.001$ and $\Delta t = 0.0001$ in (c) and (d), respectively.

$$G_{21} = \frac{1}{2}(-\bar{u}\bar{v} - gw + p\bar{u}_y + qg_y), \tag{47h}$$

$$G_{22} = -\frac{\beta}{4}(p^2 + q^2)^2 - \frac{1}{2}(\bar{v}^2 + w^2) - \frac{1}{2}(qp_t - pq_t) - \frac{1}{2}(p\bar{u}_x + qg_x). \tag{47i}$$

Having computed these physically important quantities, they are then substituted into the equations for the energy conserved quantity (equation (48)) and the momentum conserved quantities (equations (49) and (50))

$$\frac{\partial E}{\partial t} + \frac{\partial F_1}{\partial x} + \frac{\partial F_2}{\partial y} = 0, \tag{48}$$

$$\frac{\partial I_1}{\partial t} + \frac{\partial G_{11}}{\partial x} + \frac{\partial G_{12}}{\partial y} = 0, \tag{49}$$

$$\frac{\partial I_2}{\partial t} + \frac{\partial G_{21}}{\partial x} + \frac{\partial G_{22}}{\partial y} = 0. \tag{50}$$

We can then compute the L_2-*norms* of the residuals for the equations governing respectively the time varying physical quantities E, I_1 and I_2. According to Fig. 18, the proposed numerical scheme is shown to be applicable to solve the two-dimensional NLS equation.

Table 2
Comparison of the L_2- and L_∞-*error norms* computed at different grid spacings. The values shown in (•) are the computed rates of convergence. Note that (a), (b) represent the error norms computed in [26] and computed by the current scheme, respectively.

N	L_2-error norms			
	$\Re(\psi) \equiv p$		$\Im(\psi) \equiv q$	
	(a)	(b)	(a)	(b)
10	0.62	2.3824E−02	0.62	2.7514E−02
20	0.15 (2.05)	1.9139E−03 (3.63)	0.15 (2.05)	2.2341E−03 (3.62)
40	3.67E−02 (2.03)	1.2902E−04 (3.89)	3.67E−02 (2.03)	1.5065E−04 (3.89)
80	9.14E−03 (2.01)	1.9484E−05 (2.73)	9.14E−03 (2.01)	2.1317E−05 (2.82)
N	L_∞-error norms			
	$\Re(\psi) \equiv p$		$\Im(\psi) \equiv q$	
	(a)	(b)	(a)	(b)
10	0.14	6.0535E−02	0.14	8.3842E−02
20	3.34E−02 (2.07)	4.4093E−03 (3.78)	3.34E−02 (2.07)	6.6086E−03 (3.67)
40	8.25E−03 (2.02)	3.2547E−04 (3.76)	8.25E−03 (2.02)	4.5848E−04 (3.85)
80	2.06E−03 (2.00)	5.7616E−05 (2.50)	2.06E−03 (2.00)	8.0955E−05 (2.50)

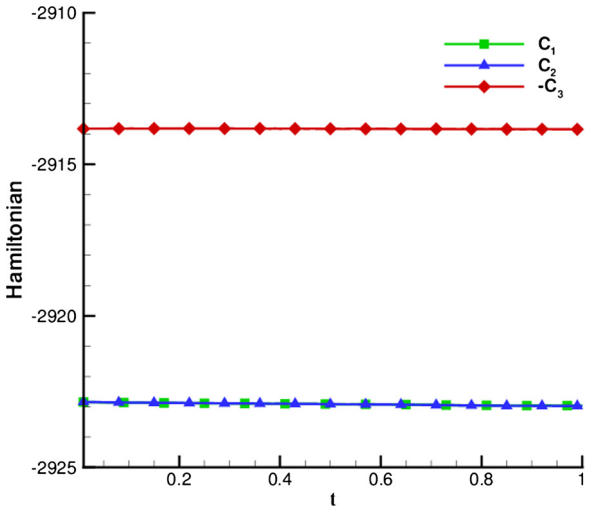

Fig. 17. The values of C_1, C_2 and $-C_3$, which are shown in equations (44)–(46), computed at $\Delta t = 0.0001$ and $\Delta x = \Delta y = \frac{2\pi}{80}$ are plotted with respect to time for $t \in [0, 1]$ and $x, y \in [0, 2\pi]$.

6. Concluding remarks

In this study a dispersion error reducing symplecticity-preserving FDTD scheme has been developed within the semi-discretization context to solve the CNLS equation in semiclassical regime. Under the small-dispersion condition, our strategy of approximating the spatial derivative term is to minimize the discrepancy between the numerical and exact dispersion relation equations for this nonlinear Hamiltonian equation. A long-time accurate simulation of the CNLS equation requires predicting the results that should satisfy the discrete Hamiltonians. The four-stage explicit symplectic time integrator of fourth-order temporal accuracy is applied. Both of the Fourier stability analysis and the modified equation analysis of second kind for the proposed explicit symplectic PRK scheme accommodating the optimized numerical dispersion relation equation have been conducted. The method of fractional steps is adopted to split the two-dimensional NLS equation into two single-dimensional equations. Through the splitting of CNLS equation, the proposed one-dimensional symplectic scheme with the optimized numerical dispersion relation equation can be applied to solve the two-dimensional Schrödinger equation.

Appendix A. Stability analysis on the proposed scheme

Since the nonlinear part of the CNLS equation (17) is amenable to exact solution, the stability condition to be derived for the proposed explicit symplecticity- and dispersion-relation-equation-preserving scheme has only association with the linear part of the Schrödinger equation, or (16), under current investigation. The stability condition will be derived below in detail.

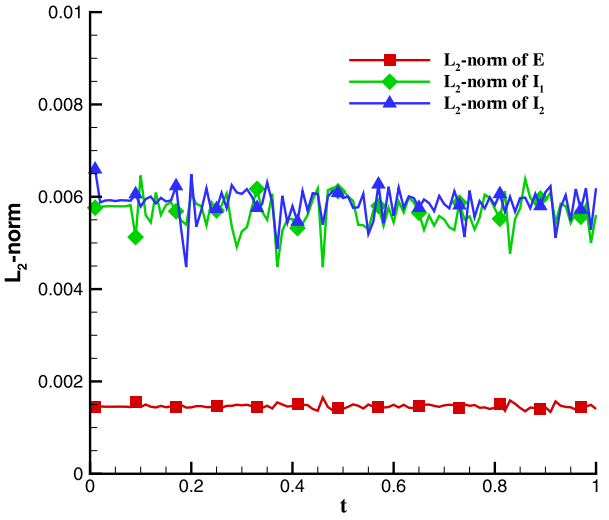

Fig. 18. The L_2-*norms* of the conservation laws for E, I_1, I_2 (equations (48)–(50)) are plotted with respect to time for the solutions predicted at $\Delta t = 0.0001$ and $\Delta x = \Delta y = \frac{2\pi}{80}$ for $t \in [0, 1]$ and $x, y \in [0, 2\pi]$.

When conducting Von Neumann stability analysis, one has to transform equation (28) from time domain to frequency domain through the discrete Fourier decomposition, which is defined as

$$\begin{aligned} \psi_i^n &= \psi_i^n, \\ \psi_i^{n+\frac{1}{2}} &= e^{-\imath\omega\frac{\Delta t}{2}}\psi_i^n, \\ \psi_{i\pm m, j\pm n}^n &= e^{\pm\imath(mk_x\Delta x + nk_y\Delta y)}\psi_i^n. \end{aligned} \tag{A.1}$$

By substituting the equations in (A.1) into equation (20), we have

$$\psi_{xx}|_i = \frac{2\gamma\cos(2k\Delta x) + 2(1-4\gamma)\cos(k\Delta x) + (6\gamma - 2)}{\Delta x^2}\psi_i \equiv \frac{A}{\Delta x^2}\psi_i. \tag{A.2}$$

The set of the high-order spatial discrete derivative terms shown in equation (28) can be similarly represented in the frequency domain by means of $\psi_{xxxx}|_i \equiv \frac{A^2}{\Delta x^4}\psi_i$, $\psi^{(6)}|_i \equiv \frac{A^3}{\Delta x^6}\psi_i$, $\psi^{(8)}|_i \equiv \frac{A^4}{\Delta x^8}\psi_i$, $\psi^{(10)}|_i \equiv \frac{A^5}{\Delta x^{10}}\psi_i$, and $\psi^{(12)}|_i \equiv \frac{A^6}{\Delta x^{12}}\psi_i$, where $A = 2\gamma\cos(2k\Delta x) + 2(1-4\gamma)\cos(k\Delta x) + (6\gamma - 2)$ and the coefficient γ has been determined in Section 3.1.2. Note that $\psi^{(n)}$ denotes the discrete expression of $\frac{\partial^n\psi}{\partial x^n}|_{t=n\Delta t}$.

The amplification factor G ($\equiv \psi_i^{n+\frac{1}{2}}/\psi_i^n$) can be then derived as follows by substituting equation (A.1) into equation (28)

$$G \equiv \frac{\psi_i^{n+\frac{1}{2}}}{\psi_i^n} = 1 + \imath CrA - \frac{Cr^2}{2!}A^2 - \imath\frac{Cr^3}{3!}A^3 + \frac{Cr^4}{4!}A^4 - \imath 0.09585Cr^5A^5 + 0.06475Cr^6A^6. \tag{A.3}$$

The necessary and sufficient condition for the proposed scheme to be conditionally stable is that the absolute value of the amplification factor $|G|$ is equal to or less than one. The amplification factor for $|G| \le 1$ is plotted with respect to Cr in Fig. 4.

By virtue of the four-stage fourth-order accurate explicit Partitioned Runge–Kutta (PRK) scheme, the linear part of the two dimensional Schrödinger equation (35) can be rewritten as

$$\begin{aligned} \imath\psi^{n+\frac{1}{2}} = {} & \imath\psi^n - \Delta t(\psi_{yy}^n + \psi_{xx}^n) - \imath\frac{\Delta t^2}{2!}(\psi_{yyyy}^n + 2\psi_{xxyy}^n + \psi_{xxxx}^n) \\ & + \frac{\Delta t^3}{3!}(\psi_{y^6} + 3\psi_{x^2y^4} + 3\psi_{x^4y^2} + \psi_{x^6}) + \imath\frac{\Delta t^4}{4!}(\psi_{y^8} + 4\psi_{x^2y^6} + 6\psi_{x^4y^4} + 4\psi_{x^6y^2} + \psi_{x^8}) \\ & + 0.01977\Delta t^5(\psi_{y^{10}} + 5\psi_{x^2y^8} + 10\psi_{x^4y^6} + 10\psi_{x^6y^4} + 5\psi_{x^8y^2} + \psi_{x^{10}}) \\ & + \imath 0.06475\Delta t^6(\psi_{y^{12}} + 6\psi_{x^2y^{10}} + 15\psi_{x^4y^8} + 20\psi_{x^6y^6} + 15\psi_{x^8y^4} + 6\psi_{x^{10}y^2} + \psi_{x^{12}}). \end{aligned} \tag{A.4}$$

Note that $\psi_{x^n y^m}$ is denoted as the discrete expression of $\frac{\partial^n}{\partial x^n}\frac{\partial^m}{\partial y^m}\psi^n|_{t=n\Delta t}$. Following the similar derivation procedures described above, the derived amplification factor G $(\equiv \psi_i^{n+\frac{1}{2}}/\psi_i^n)$ under $\Delta x = \Delta y$ is given below, where Cr_x $(\equiv \frac{\Delta t}{\Delta x^2})$ $= Cr_y$ $(\equiv \frac{\Delta t}{\Delta y^2}) = Cr$

$$\begin{aligned} G \equiv \frac{\psi_i^{n+\frac{1}{2}}}{\psi_i^n} &= 1 + \imath Cr(A+B) - \frac{Cr^2}{2!}(A^2+2AB+B^2) \\ &\quad - \imath\frac{Cr^3}{3!}(A^3+3A^2B+3AB^2+B^3) + \frac{Cr^4}{4!}(A^4+4A^3B+6A^2B^2+4AB^3+B^4) \\ &\quad - \imath 0.09585Cr^5(A^5+5A^4B+10A^3B^2+10A^2B^3+5AB^4+B^5) \\ &\quad + 0.06475Cr^6(A^6+6A^5B+15A^4B^2+20A^3B^3+15A^2B^4+6AB^5+B^6). \end{aligned} \tag{A.5}$$

In the above, A and B are as follows

$$\begin{aligned} A &= 2\gamma\cos(2k\Delta x) + 2(1-4\gamma)\cos(k\Delta x) + (6\gamma-2), \\ B &= 2\gamma\cos(2k\Delta y) + 2(1-4\gamma)\cos(k\Delta y) + (6\gamma-2). \end{aligned} \tag{A.6}$$

The coefficient γ has been determined by minimizing the discrepancy between the numerical and exact dispersion relation equation for the two-dimensional case. As Fig. 5 shows, the magnitudes of the amplification factor $|G|$ approaches one as Cr decreases. One can also see clearly that calculation of the two-dimensional stable solution suffers a comparatively stringent stability condition.

References

[1] A. Hasegawa, Y. Kodama, Solitons in Optical Communications, Oxford, Clarendon Press, 1995.
[2] T.B. Benjamin, J.E. Feir, The disintegration of wave trains on deep water. Part 1. Theory, J. Fluid Mech. 27 (3) (1967) 417–430.
[3] J.B. Chen, M.Z. Qin, Y.F. Tang, Symplectic and multi-symplectic methods for the nonlinear Schrödinger equation, Comput. Math. Appl. 43 (2002) 1095–1106.
[4] S. Reich, Multi-symplectic Runge–Kutta collocation methods for Hamiltonian wave equations, J. Comput. Phys. 157 (2000) 473–499.
[5] X.S. Liu, Y.Y. Qi, J.F. He, P.Z. Ding, Recent progress in symplectic algorithm for use in quantum systems, Commun. Comput. Phys. 2 (1) (2007) 1–53.
[6] L. Lee, G. Lyng, I. Vankova, The Gaussian semiclassical soliton ensemble and numerical methods for the focusing nonlinear Schrödinger equation, Physica D 241 (2012) 1767–1781.
[7] G.P. Agrawal, Nonlinear Fiber Optics, 2nd edition, Academic Press, San Diego, California, 1995.
[8] T.B. Benjamin, K. Hasselmann, Instability of periodic wave trains in nonlinear dispersive systems, Proc. R. Soc. Lond. Ser. A, Math. Phys. Sci. 299 (1456) (1967) 59–76.
[9] W. Bao, S. Jin, P.A. Markowich, On time-splitting spectral approximations for the Schrödinger equation in the semiclassical regime, J. Comput. Phys. 175 (2002) 487–524.
[10] P.A. Markowich, P. Pietra, C. Pohl, Numerical approximation of quadratic observables of Schrödinger equations in the semi-classical limit, Numer. Math. 81 (1999) 595–630.
[11] C. Heitzinger, C. Ringhofer, A note on the symplectic integration of the nonlinear Schrödinger equation, J. Comput. Electron. 3 (1) (2004) 33–44.
[12] Z. Rapti, P.G. Kevrekidis, D.J. Frantzeskakis, B.A. Malomed, On the modulational instability of the nonlinear Schrödinger equation with dissipation, Phys. Scr. T 113 (2004) 74–77.
[13] G. Fibich, Self-focusing in the damped nonlinear Schrödinger equation, SIAM J. Appl. Math. 61 (15) (2001) 1680–1705.
[14] T.J. Bridges, Multi-symplectic structures and wave propagation, Math. Proc. Camb. Philos. Soc. 121 (1997) 147–190.
[15] T.J. Bridges, S. Reich, Numerical methods for Hamiltonian PDEs, J. Phys. A, Math. Gen. 39 (2006) 5287–5320.
[16] X.S. Liu, L.W. Su, P.Z. Ding, Symplectic algorithm for use in computing the time-independent Schrödinger equation, Int. J. Quant. Chem. 87 (1) (2002) 1–11.
[17] X. Liu, Y.C. Sun, Y. Tang, Conservativity of symplectic methods for the Ablowitz–Ladik discrete nonlinear Schrödinger equation, Master thesis, Chinese Academy of Science, 2004.
[18] V.E. Zakharov, A.B. Shabat, Interaction between solitons in a stable medium, Sov. Phys. JETP 64 (1973) 1627–1639.
[19] A. Aydin, B. Barasözen, Symplectic and multi-symplectic methods for coupled nonlinear Schrödinger equations with periodic solutions, Comput. Phys. Commun. 177 (2007) 566–583.
[20] T.J. Bridges, S. Reich, Multi-symplectic integrators: numerical schemes for Hamiltonian PDEs that conserves symplecticity, Phys. Lett. A 284 (2001) 184–193.
[21] E. Hairer, C. Lubich, G. Wanner, Geometric Numerical Integration: Structure-Preserving Algorithms for Ordinary Differential Equations, 2nd edition, Springer Ser. Comput. Math., vol. 31, 2006.
[22] W. Bao, S. Jin, P.A. Markowich, Numerical study of time-splitting spectral discretizations of nonlinear Schrödinger equations in the semiclassical regimes, SIAM J. Sci. Comput. 25 (1) (2003) 27–64.
[23] J.M. Sanz-Serna, A. Portillo, A classical numerical integrators for wave-packet dynamics, J. Chem. Phys. 104 (6) (1996) 2349–2355.
[24] C.K.W. Tam, J.C. Webb, Dispersion–relation-preserving finite difference schemes for computational acoustics, J. Comput. Phys. 107 (1993) 262–281.
[25] N.N. Yanenko, in: M. Holt (Ed.), The Methods of Fractional Steps: The Solution of Problems of Mathematical Physics in Several Variables, Springer-Verlag, New York, 1971.
[26] Y.M. Chen, H.J. Zhu, S.H. Song, Multi-symplectic splitting method for two-dimensional nonlinear Schrödinger equation, Commun. Theor. Phys. 56 (2011) 617–622.
[27] Q. Chang, E. Jia, W. Sun, Difference schemes for solving the generalized nonlinear Schrödinger equation, J. Comput. Phys. 148 (1999) 397–415.
[28] S. Jin, C.D. Levermore, D.W. McLaughlin, Singular Limits of Dispersive Waves: The Behavior of Solutions of the NLS Equation in the Semiclassical Limit, Plenum Press, New York and London, 1994.
[29] J.C. Bronski, D.W. McLaughlin, Singular Limits of Dispersive Waves: Semiclassical Behavior in the NLS Equation: Optical Shocks-focusing Instabilities, Plenum Press, New York and London, 1994.
[30] S. Jin, C.D. Levermore, D.W. McLaughlin, The semiclassical limit of the defocusing NLS hierarchy, Commun. Pure Appl. Math. 52 (5) (1999) 613–654.